

University of Windsor

Scholarship at UWindor

Electronic Theses and Dissertations

Theses, Dissertations, and Major Papers

2004

Drive control and real-time simulation for switched reluctance motor in a fuel cell power system.

Meranda Salem
University of Windsor

Follow this and additional works at: <https://scholar.uwindsor.ca/etd>

Recommended Citation

Salem, Meranda, "Drive control and real-time simulation for switched reluctance motor in a fuel cell power system." (2004). *Electronic Theses and Dissertations*. 1783.
<https://scholar.uwindsor.ca/etd/1783>

This online database contains the full-text of PhD dissertations and Masters' theses of University of Windsor students from 1954 forward. These documents are made available for personal study and research purposes only, in accordance with the Canadian Copyright Act and the Creative Commons license—CC BY-NC-ND (Attribution, Non-Commercial, No Derivative Works). Under this license, works must always be attributed to the copyright holder (original author), cannot be used for any commercial purposes, and may not be altered. Any other use would require the permission of the copyright holder. Students may inquire about withdrawing their dissertation and/or thesis from this database. For additional inquiries, please contact the repository administrator via email (scholarship@uwindsor.ca) or by telephone at 519-253-3000ext. 3208.

DRIVE CONTROL AND REAL TIME SIMULATION FOR
SWITCHED RELUCTANCE MOTOR IN A FUEL CELL
POWER SYSTEM

BY

MERANDA SALEM

A thesis

Submitted to the Faculty of Graduate Studies and Research
through Electrical and Computer Engineering in Partial
Fulfillment of the Requirements for the Degree of Master of
Applied Science at the University of Windsor

Windsor, Ontario, Canada

2004

@ 2004 Meranda Salem



Library and
Archives Canada

Bibliothèque et
Archives Canada

Published Heritage
Branch

Direction du
Patrimoine de l'édition

395 Wellington Street
Ottawa ON K1A 0N4
Canada

395, rue Wellington
Ottawa ON K1A 0N4
Canada

Your file Votre référence

ISBN: 0-494-00141-0

Our file Notre référence

ISBN: 0-494-00141-0

NOTICE:

The author has granted a non-exclusive license allowing Library and Archives Canada to reproduce, publish, archive, preserve, conserve, communicate to the public by telecommunication or on the Internet, loan, distribute and sell theses worldwide, for commercial or non-commercial purposes, in microform, paper, electronic and/or any other formats.

The author retains copyright ownership and moral rights in this thesis. Neither the thesis nor substantial extracts from it may be printed or otherwise reproduced without the author's permission.

AVIS:

L'auteur a accordé une licence non exclusive permettant à la Bibliothèque et Archives Canada de reproduire, publier, archiver, sauvegarder, conserver, transmettre au public par télécommunication ou par l'Internet, prêter, distribuer et vendre des thèses partout dans le monde, à des fins commerciales ou autres, sur support microforme, papier, électronique et/ou autres formats.

L'auteur conserve la propriété du droit d'auteur et des droits moraux qui protègent cette thèse. Ni la thèse ni des extraits substantiels de celle-ci ne doivent être imprimés ou autrement reproduits sans son autorisation.

In compliance with the Canadian Privacy Act some supporting forms may have been removed from this thesis.

Conformément à la loi canadienne sur la protection de la vie privée, quelques formulaires secondaires ont été enlevés de cette thèse.

While these forms may be included in the document page count, their removal does not represent any loss of content from the thesis.

Bien que ces formulaires aient inclus dans la pagination, il n'y aura aucun contenu manquant.


Canada

Drive control and Real time simulation for Switched Reluctance Motor in a
fuel cell power system

by

Meranda Salem

APPROVED BY:

B. Zhou


Mechanical Engineering

 K. Tepe

Electrical and Computer Engineering

X. Chen, Advisor

~~Electrical~~ and ~~Computer~~ Engineering

 Dr. M. Sid-Ahmed, Chair of Defense

Electrical and Computer Engineering

09/24/04

ABSTRACT

DRIVE CONTROL AND REAL TIME SIMULATION FOR SWITCHED RELUCTANCE MOTOR IN A FUEL CELL POWER SYSTEM

Switched Reluctance Motor (SRM) drive is considered as a possible alternative to other conventional variable-speed drives because of several advantages [1], [2]. However, in order for the performance of a switched reluctance motor drive to suit several applications, it has to be tailored through appropriate control.

Rotor position sensing is an integral part of SRM control because of the nature of torque production. Sensorless control reduces overall cost and dimension of the drive in addition to improving reliability.

In this thesis, an Inductance Model Based Sensorless [8] Switched Reluctance Motor is used to design the drive controller for SRM. A hysteresis current controller and a speed controller were implemented to produce smooth torque and a stable speed for SRM. In addition, the dc power supply for the SRM was derived from Fuel Cell Stack rather than from batteries or from utility lines through a front-end diode rectifier.

In this research, first, the current controller and the speed controller are developed and connected to the Inductance Based Sensorless SRM model with the Fuel Cell Stack model and an offline simulation using Matlab/Simulink is obtained. A detailed computer model of the SRM control drive connected to the

Fuel Cell stack model is developed in which the design of the proposed controller scheme is verified.

As a next major step, a Real-Time simulation was obtained for the model using Opal-RT platform, and a comparison between the offline simulation results and real time simulation results is developed. As a final step, the characteristics of the SRM Inductance model, Controller model, and the Fuel Cell stack model are studied in detail, which is required in order to use them in future applications.

ACKNOWLEDGMENTS

I would like to express my appreciation to Dr. X. Chen for his inspiring guidance, constant encouragement and simulating suggestions throughout the progress of this work. I also would like to extend my thanks to my mom Dr. Nadia Ibrahim, and to all my brothers and sisters for their support. I am also thankful to Mr. Tuhin K. Das from Emmeskay Inc., and to Mr. Alan Soltis from Opal-RT for their invaluable assistance. Moreover, my sincere thanks to the members of my committee for their interest in this project and to Mr. Marc Trepanier, my boss at Current Engineering Ltd. For his help and support during my master studies. Finally and most of all I would like to Thank God for helping me and supporting me and giving me the strength and knowledge and all of the above mentioned names to be able to success in this research.

TABLE OF CONTENTS

ABSTRACT	iii
ACKNOWLEDGMENTS	v
LIST OF FIGURES	ix
CHAPTER 1 : INTRODUCTION	1
1.1 RESEARCH GOALS	1
1.2 CONTROL OF THE SWITCHED RELUCTANCE MOTOR	2
1.3 SWITCHED RELUCTANCE MOTOR	5
1.4 FUEL CELL STACK	7
1.5 THESIS ORGANIZATION	11
CHAPTER 2 : SWITCHED RELUCTANCE MODEL AND FUEL CELL STACK MODEL	13
2.1 SWITCHED RELUCTANCE MOTOR MODEL (SRM)	13
2.1.1 STATIC CHARACTERISTICS OF THE SRM	14
2.1.2 TORQUE PRODUCTION MECHANISM IN SRM DRIVES	16
2.1.3 SRM CHOPPER TOPOLOGIES	18
2.1.4 THEORY OF THE SRM INDUCTANCE MODEL	23
A. DYNAMIC EQUATIONS OF THE SRM DRIVE	24
B. DERIVATION OF THE SRM INDUCTANCE MODEL	26
2.2 FUEL CELL STACK MODEL	31
2.2.1 SYSTEM INTERACTIONS	33
A. REACTANT FLOW SUBSYSTEM	34

B. HEAT AND TEMPERATURE SUBSYSTEM	34
C. WATER MANAGEMENT SUBSYSTEM	35
D. POWER MANAGEMENT SUBSYSTEM	35
E. FUEL PROCESSOR SUBSYSTEM	36
2.2.2 FUEL CELL STACK MODEL	37
CHAPTER 3: SRM DRIVE CONTROLLER	39
3.1 FORMULATION OF THE SENSORLESS ALGORITHM	41
3.1.1 LOW SPEED OPERATION	42
3.1.2 HIGH SPEED OPERATION	43
3.2 COMMUTATION ANGLE CONTROLLER	43
3.3 HYSTERESIS CURRENT CONTROLLER	45
3.3.1 HYSTERESIS CURRENT CONTROLLER THEORY	47
3.3.2 COMMUTATION PROCEDURE	51
3.4 PI – SPEED CONTROLLER	52
3.4.1 PERFORMANCE AND SPECIFICATIONS	53
3.4.2 SPEED CONTROLLER	54
CHAPTER 4:	
SIMULINK MODEL IMPLEMENTATION AND OFF-LINE AND REAL-TIME SIMULATION	59
4.1 DYNAMIC EQUATIONS OF THE SRM DRIVE	59
4.2 DESCRIPTION OF THE DYNAMIC MODEL OF THE SRM CONTROL DRIVE	62
4.3 HYSTERESIS CONTROLLER	65
4.4 PI SPEED CONTROLLER	66

4.5 OFFLINE SIMULATION RESULTS	67
4.6 REAL-TIME SIMULATION	70
4.6.1 COMMAND STATION	71
4.6.2 TARGET NODES	71
4.6.3 COMPILATION NODE	72
4.6.4 COMMUNICATION	72
4.6.4.1 FIREWIRE REAL-TIME LINK	72
4.6.4.2 ETHERNET LINK	73
4.6.4.3 I/O BOARDS	73
4.7 REAL-TIME SIMULATION FOR SRM DRIVE CONTROL	73
4.7.1 RUNNING SRM DRIVE CONTROL IN RT-LAB SOFTWARE	75
CHAPTER 5: SUMMARY AND CONCLUSIONS	80
5.1 INTRODUCTION	80
5.2 SUMMARY OF THE THESIS	81
5.3 ADVANTAGES AND DISADVANTAGES OF P-I CONTROLLER	82
5.4 SUGGESTIONS FOR FUTURE WORK	83
REFERENCES	85
APPENDIX A	91
APPENDIX B	96

LIST OF FIGURES

FIGURE	PAGE
FIGURE 1.1: SRM CROSS SECTION	6
FIGURE 1.2: FUEL CELL CHEMICAL REACTION	9
FIGURE 2.1: FLUX-LINKAGE AS A FUNCTION OF STATOR PHASE CURRENT AND ROTOR POSITION	15
FIGURE 2.2: STORED FIELD ENERGY AND COENERGY	17
FIGURE 2.3: SRM CLASSIC CHOPPER	18
FIGURE 2.4: MODES OF OPERATION FOR ONE PHASE OF THE SRM CHOPPER	19
FIGURE 2.5: SRM CLASSIC CHOPPER USING POWER MOSFETS	20
FIGURE 2.6: C-DUMP CHOPPER	21
FIGURE 2.7: THREE DIFFERENT TYPES OF SRM CHOPPER	22
FIGURE 2.8: VARIATION OF INDUCTANCE AT THE ALIGNED POSITION WITH CURRENT	29
FIGURE 2.9: FUEL CELL SYSTEM	32
FIGURE 2.10: FUEL SOURCES FOR FUEL CELL SYSTEMS	37
FIGURE 3.1: FIRING ANGLES VARY WITH ROTOR SPEED	44
FIGURE 3.2: HYSTERESIS CURRENT CONTROLLER BLOCK DIAGRAM	45
FIGURE 3.3: OPERATIONAL WAVEFORM	46
FIGURE 3.4: IDEAL CURRENT WAVEFORM FOR DERIVING THE HYSTERESIS CURRENT CONTROLLER EQUATION	48
FIGURE 3.5: BLOCK DIAGRAM FOR THE CURRENT CONTROLLER METHOD	51

FIGURE 4.1: BLOCK SCHEMATIC OF THE SRM DRIVE CONTROL SYSTEM USED FOR SIMULATION	63
FIGURE 4.2: SPEED CONTROLLER BLOCK DIAGRAM	67
FIGURE 4.3: FOUR PHASE SRM CURRENT OFFLINE SIMULATION	68
FIGURE 4.4: TORQUE OFFLINE SIMULATION BEFORE ADDING THE SPEED CONTROLLER	68
FIGURE 4.5: SPEED OFFLINE SIMULATION BEFORE ADDING THE SPEED CONTROLLER	69
FIGURE 4.6: TORQUE OFFLINE SIMULATION AFTER ADDING THE SPEED CONTROLLER	69
FIGURE 4.7: SPEED OFFLINE SIMULATION AFTER ADDING THE SPEED CONTROLLER	69
FIGURE 4.8: REAL-TIME FOUR PHASE SRM CURRENT	76
FIGURE 4.9: TORQUE REAL TIME SIMULATION (ZOOMED IN AREA) BEFORE ADDING SPEED CONTROLLER	77
FIGURE 4.10: TORQUE REAL TIME SIMULATION (ZOOMED OUR AREA) BEFORE ADDING SPEED CONTROLLER	77
FIGURE 4.11: SPEED REAL TIME SIMULATION (ZOOMED IN AREA) BEFORE ADDING SPEED CONTROLLER	78
FIGURE 4.12: SPEED REAL TIME SIMULATION (ZOOMED OUT AREA) BEFORE ADDING SPEED CONTROLLER	78
FIGURE 4.13: TORQUE REAL TIME SIMULATION AFTER ADDING SPEED CONTROLLER	78
FIGURE 4.14: SPEED REAL TIME SIMULATION AFTER ADDING SPEED CONTROLLER	79
FUEL CELL STACK SIMULINK MODEL	96
SRM DRIVE CONTROL SIMULINK MODEL	96
SRM INDUCTANCE MODEL DEVELOPED IN DR. EHSANI'S WORK	97
SRM POWER CHOPPER SIMULINK MODEL	97

SIMULINK MECHANICAL MODEL	98
COMMUTATOR ANGLE SIMULINK MODEL	98
DC/DC CONVERTER SIMULINK MODEL	98
CURRENT CONVERTER SIMULINK MODEL	99
HYSTERESIS CURRENT CONTROLLER SIMULINK MODEL	100
PI SPEED CONTROLLER SIMULINK MODEL	100

CHAPTER 1

INTRODUCTION

1.1 Research Goals

The ultimate two goals for the project is to design and apply a controller based on the Proportional-Integral control strategy in the speed control of the Switched Reluctance Motor powered by a Fuel Cell system, and to simulate the proposed speed control system in a Real-time Simulation and also to investigate the performance and report on the results. Several drive control methods for SRM have been reported in literature in the last decade. The various drive control methods published in literature can be broadly classified into the following: Sensorless control method using mechanical position sensor [3], [4], Fuzzy logic control method [5], Artificial intelligence control [6], Fixed angle control [7] etc. The various methods suggested in literature have their own merits and demerits depending on their principles of operation. Ideally, it is desirable to have a drive control scheme which smoothes both the SRM torque and speed and does not require complicated nonlinear system to design it.

In this research, a new SRM drive control method using Hysteresis Current Controller and PI Speed Controller is developed. The proposed drive control scheme relies on the inductance model of the SRM drive using the four phases currents as a feedback to the Hysteresis current controller and the speed of the motor as the feedback to the PI speed controller. This chapter will give a brief introduction for the SRM and the Fuel Cell system. In the following chapters the SRM model, Fuel Cell model, and the proposed drive controller model will be

explained in details as well as the offline simulation and the real time simulation results.

1.2 Control of The Switched Reluctance Motor

Control of the motor is made more complicated by the nonlinearities found not only in the motor, but also in the switching choppers, which arise due to the power switches. Most of the literature on Switched Reluctance Motor drives focuses on the design and modeling of the motor and on the configuration of power choppers. There are several papers that address the control aspects of the SRM.

Open-loop strategies have been suggested and investigations using angle and current amplitude regulation were reported. Use of constant input voltage [64] is the simplest and most commonly used control strategy for the SRM. The phases are turned off and on based on the switching imposed by the electronic commutator. Since this is an open-loop control strategy, a better design of the motor itself and its electronic commutator can only achieve improvement of the dynamic behavior. Such a scheme suffers from the fact that the response is not robust when the motor is exposed to internal or external disturbances.

Closed-loop control strategies for switched reluctance motors are proposed in [64-68]. [64] introduced for the first time the application of feedback linearization to electric drives. They reported the work on control of SRM for trajectory tracking in robotics applications. In this work they developed a nonlinear mathematical model based on experimentally measured data. It is assumed that all plant parameters are known and that the motor acceleration is

measurable. Unfortunately, their controller is computationally quite complex and, moreover, requires the accurate model of external loads in addition to that of the SRM.

In [65], the equations of the SRM are expressed in a rotating reference frame. Constant speed as well as piecewise linearized inductance curves and known parameters are assumed. However instantaneous torque control is taken into account, while magnetic saturation is ignored. The paper shows that, under the assumption of constant velocity, the SRM may be modeled as a linear time-varying system. This design gives good results only for SRM operating at low speed. Moreover, a tradeoff is considered between peak torque and torque ripple.

In [66] a fuzzy logic controller is used to control the speed of a SRM drive. Fuzzy logic controllers are based on the theory of fuzzy sets and fuzzy logic. The design of a fuzzy logic controller does not require an accurate model of the plant, which is appreciated in motor drive applications where the motor and/or the mechanical load are usually described by a set of nonlinear differential equations or are partially unknown. A conventional controller adjusts the system control parameters on the basis of a set of differential equations, which represents a model of the process dynamics. In a fuzzy logic controller, these adjustments are handled by a fuzzy rule-based expert system. While the overall fuzzy behavior avoids any speed overshoot, the ripples usually related to the switching are still unavoidable.

In [67] a model-reference adaptive control of a variable reluctance motor for low speed, high speed mode of operation suitable for robotics applications has been considered. This model leads to an adaptive controller. This work concerns itself only with the low-speed operation. In this study, instead of using the full order system, a reduced-order model is considered. The paper also assumes that the magnetic saturation is due to the winding current only and is not a function of the rotor position.

In [68] the design of a feedback linearization controller for SRM is presented. The mathematical model of the motor takes the magnetic saturation into account. The main idea behind the feedback linearization control scheme is to transform the nonlinear system dynamics into a linear one.

[69] examines the feasibility of using artificial neural networks to develop discrete time dynamic models for a SRM drive system that includes both faulty and fault-free behaviors. The purpose of this work is to present a methodology that can be used to construct an artificial neural network capable of modeling the dynamics of SRM drive systems, or any dynamical systems. The approach employed in this paper, however, appears to consume considerable computational resources.

While proportional-integral control scheme represents a simple strategy, its implementation for driving an SRM is rather novel, and its good performance is apparent. In the competition with more advanced controller, the P-I controller has generally been regarded as one of the most likely candidates to succeed in industrial applications. The main reasons for this include: simplicity, lower cost,

ability to achieve zero steady-state error, ease of implementation, robustness, good speed of response, good stability, and other desirable features. P-I controllers are extensively used in many drives where speed control is desired. In this thesis, a speed controller based on the proportional-integral control strategy is used.

1.3 Switched Reluctance Motor

Switched Reluctance Motor (SRM) drive has considered as a possible alternative in several variable speed applications because of its advantages [1], [2]. Rugged and simple construction, inherent variable speed capability, ease of control, etc. are some of the positive aspects of the SRM drive. Switched Reluctance Motor drives are being tried in aircraft starter/generator systems, automotive and home appliance applications.

SRM drives are also known for their fault tolerant operation. The rotor construction is very rugged and does not have windings or permanent magnets on it, which allows very high speed operation possible without much concern about the centrifugal forces. In the chopper side, since the phase windings are connected in series with the upper and lower switches, shoot-through fault does not happen in case one of the switches is shorted.

There are also few disadvantages of SRM drives, such as high level of acoustic noise [9]-[11] and torque ripple [12], [13] especially at low operating speeds, need for mechanical position sensor, etc.

SRM is a doubly salient, singly excited machine with unequal number of stator and rotor poles [1], [2]. Most common stator to rotor pole configuration is

6:4 and 8:6. The stator poles have concentrated windings and the coils on diametrically opposite poles are connected either in series or parallel to form one phase group.

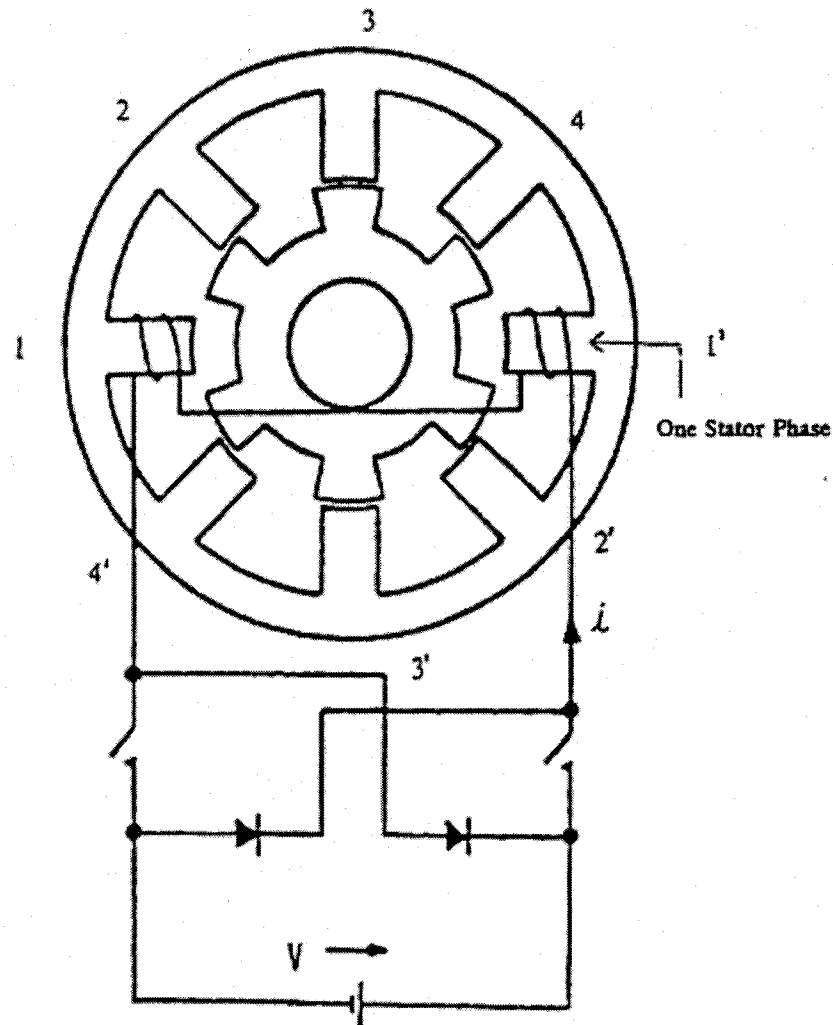


Figure 1.1: SRM Cross-Section

The above figure illustrates the cross-sectional view of an 8/6, four phases SRM with only one switching circuit for only one phase. The rotor poles are made of magnetic steel laminations and do not carry windings or permanent magnets. The rotor has a robust construction and is suitable for very high-speed application without any need for mechanical gears [14].

In SRM, the torque is produced by the tendency of the rotor poles to align with the stator pole pairs that are energized. The energization of a pair of stator coils will attract a pair of rotor poles that are nearest to the corresponding stator poles. Thus, a sequential energization of the coils in the stator phases will result in continuous torque production causing the rotor to rotate [15].

For smooth rotation it is necessary to energize the SRM stator phases in synchronism with the reluctance variation, or in other words, in synchronism with the rotor position. A power chopper is used for achieving this, which basically controls the magnitude and timing of the stator phase currents. By controlling the magnitude and timing of the stator phase currents with reference to the rotor position, effective variable speed operation of the drive is thus achieved. The SRM inductance model as well as the power chopper model will be explained in details in chapter 2.

1.4 Fuel Cell Stack

Fuel Cells are electrochemical devices that convert the chemical energy of a gaseous fuel directly into electricity and are widely regarded as a potential alternative stationary and mobile power source. They complement heat engines and reduce the ubiquitous dependence on fossil fuels and thus have significant environmental and national security implications [16].

Fuel cell stack systems are under intensive development by several manufacturers, with the Proton Exchange Membrane (PEM) Fuel Cells (also known as Polymer Electrolyte Membrane Fuel Cells) currently considered by

many to be in a relatively more developed stage for ground vehicle applications [17]. Recent announcements of GM "Autonomy" concept and federal program "Freedom CAR" confirm an interest in developing fuel cell vehicles from both the government and automobile manufacturers [18].

To compete with ICE engines, however, fuel cell system must operate and function at least as well as conventional engines. Transient behavior is one of the key requirements for the success of fuel cell vehicles. The fuel cell system power response depends on the air and hydrogen feed, flow and pressure regulation, and heat and water management. During transient, the fuel cell stack control system is required to maintain optimal temperature, membrane hydration, and partial pressure of the reactants across the membrane in order to avoid degradation of the stack voltage, and thus, maintain high efficiency and extend the life of the stack [19].

The Fuel Cell principle was discovered in 1839 by a British Physicist called William R. Grove [20]. A fuel cell consists of an electrolyte sandwiched between two electrodes. The electrolyte has a special property that allows positive ions (protons) to pass through while blocking electrons. Hydrogen gas passes over one electrode, called an anode, and with the help of a catalyst, separates into electrons and hydrogen protons as shown in the following figure.

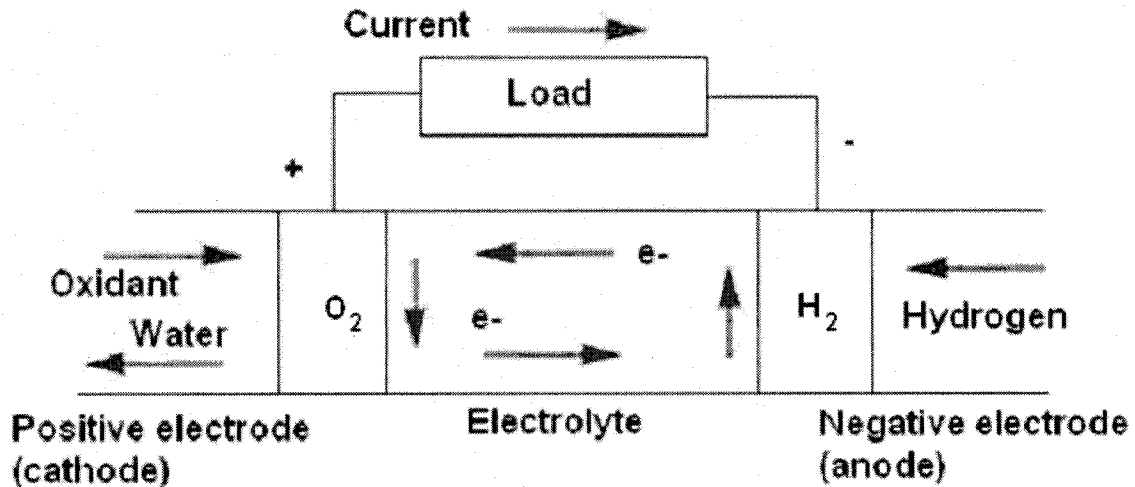
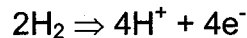
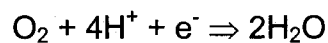


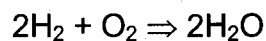
Figure 1.2: Fuel Cell Chemical Reaction



The protons flow to the other electrode, called a cathode, through the electrolyte while the electrons flow through an external circuit, thus creating electricity. The hydrogen protons and electrons combine with oxygen flow through the cathode, and produce water.



Therefore, the overall reaction of the fuel cell is



The voltage produced from one cell is between 0 to 1 volts [21] depending on fuel cell operating conditions and the size of load connected to the fuel cell. The typical value of the fuel cell voltage is about 0.7 volts. To get higher voltage, multiple cells are stacked in series. The total stack voltage can be calculated from the number of cells multiplied by the average cell voltage. There are electrical resistances in the fuel cell like other electrical devices. The loss

associated with the resistance is dissipated in the form of heat, which concludes that heat is released from the fuel cell reaction.

Fuel cells have several advantages over internal combustion engines (ICE) and batteries. To generate mechanical energy, the ICE first converts fuel energy to thermal energy by combusting fuel with oxygen at high temperature. The thermal energy is then used to generate mechanical energy. Since thermal energy is involved, the efficiency of the conversion process is limited by the Carnot Cycle [22]. On the other hand, unlike ICE, fuel cells directly convert fuel energy to electrical energy and its maximum efficiency is not subjected to Carnot Cycle limitations.

Higher energy conversion efficiency can potentially be achieved by fuel cells. If hydrogen is used as fuel, the outcome of the fuel cell reaction is water and heat. Therefore, fuel cells are considered to be a zero emission power generator. They do not create pollutants such as hydrocarbon or oxide of nitrogen. A battery is also an electrochemical device that converts chemical energy directly to electricity. However, the battery reactants are stored internally and when used up, the battery must be recharged or replaced. The reactants of fuel cell are stored externally. Oxygen is typically taken from atmospheric air and hydrogen is stored in high-pressure or cryogenic tanks, which can be refueled. Refueling tanks requires significantly less time than recharging batteries [22].

There are different types of fuel cells, distinguished mainly by the type of electrolyte used. Each type of fuel cell is suitable for different applications, because of the differences in each cell characteristics, such as cell material,

operating temperature, and fuel diversity. The Polymer Electrolyte Membrane Fuel Cells (PEMFC) are suitable for automobile applications. PEMFCs have high power density, a solid electrolyte, long life, as well as low corrosion [22]. Also PEMFCs operate in the temperature range of 50 - 100°C which allows safer operation and eliminates the need of thermal insulation. All the information presented above were a brief introduction for Fuel cell's history, advantages, uses and how it works, and the idea for using it as a power system for the SRM. Since the ultimate goal for this project is the design and modeling for the SRM drive control, a Simulink model representing the Fuel Cell stack designed by Emmeskay Inc. was used to supply the dc voltage for the SRM drive, which will be explained in detail in chapter 3.

1.5 Thesis Organization

Developing a drive control for SRM using the inductance model for the motor to achieve the current and the speed control is the central subject of this thesis. In addition, the use of Fuel Cell stack as a power system to drive the motor and running the model in real-time platform is the second main subject of this thesis.

The thesis starts with an introduction in Chapter 1 about the Switched Reluctance Motor structure, advantages, its need for drive control, and a brief survey for the various drive control methods that were presented in literature. Also this chapter gave a brief introduction about the Fuel Cell Stack history, how it works, advantages, and uses.

The theory and the method of driving the SRM inductance model are presented in Chapter 2. Also the idea of using the inductance method to model the SRM other than using other methods is explained with a comparison between the inductance method and the other methods from literature. Moreover, the electromagnetic behavior of the SRM and the torque production mechanism in SRM are examined and the choppers used for winding current commutation are presented. In addition, this chapter will present the system interactions for the fuel cell and Emmeskay's fuel cell simulink model.

Chapter 3 presents the SRM drive controller, which consists of the hysteresis current controller, commutation angle controller and the PI Speed controller. Moreover, the Offline simulation and Real time simulation for the model is presented in Chapter 4, and finally Chapter 5 gives a summary of the work done, the contribution of this research and future research in this area.

CHAPTER 2

SWITCHED RELUCTANCE MODEL AND FUEL CELL STACK MODEL

2.1 Switched Reluctance Motor Model

A power chopper and associated control system are required for Switched Reluctance Motor's (SRM) basic operation. A well designed SRM drive system matches the performance of conventional ac motor drives and it has several advantages over them. Through appropriate control, it is possible to apply SRM drives for high performance applications.

A typical SRM drive system consists of the switched reluctance motor, the power chopper and associated control system. The chopper is connected to a dc power supply, which is derived from the Fuel Cell Stack voltage. The controller energizes each phase of the SRM in a sequence and the energization is synchronized with the rotor position in order to produce smooth unidirectional torque. This necessitates a mechanical position sensor, which is usually connected to the shaft of the SRM in order to provide rotor position feedback to the controller.

The controller reads the mechanical position and decides the appropriate phase to be energized. Ideally, each stator phase is excited with a square pulse of current. The energization of one phase coil results in a magnetic force of attraction with the nearest rotor pole pair thus producing torque. The magnitude

and timing of the current pulse, in combination with the machine parameters have a direct effect on the magnitude of the torque developed [11], [23].

In order to design a control system for an SRM drive, it is essential to understand the static characteristics of the motor along with the mechanism of torque production and the commonly used chopper topologies.

2.1.1 Static Characteristics of The Switched Reluctance Motor

In the SRM, the reluctance of the magnetic flux path in a given phase changes with rotor movement. The reluctance is maximum when the stator and rotor poles are aligned and minimum when the poles are unaligned. This variation in reluctance reflects in the self-inductance of the respective stator phase. When the stator and rotor poles are aligned, the self-inductance of the stator phase will be maximum and when the poles are unaligned, the self-inductance of the phase will be minimum [23].

In order to have efficient electromechanical energy conversion, the switched reluctance motors are usually designed to operate at high levels of magnetic saturation and hence the air gap length is very small compared to other motors. The magnetic behavior of the steel lamination change with varying levels of saturation and it is reflected on the inductance as well. Thus, the stator phase inductance varies with the instantaneous phase current at any given rotor position [23].

Because of the magnetic saturation, the stator phase inductance at the aligned position varies considerably with the variation in the stator phase current.

The unaligned inductance does not vary much mainly because of the large reluctance caused due to the huge air in the flux path. Though the inductance variation with rotor position is trapezoidal in nature, in reality, the edges in the trapezoid are rounded off due to local saturation effects, thus making the inductance variation look more like a distorted sinusoid with a dc offset [23].

The flux-linkage variation with rotor position and stator phase current can also represent the static characteristics of the SRM, as shown in the following figure.

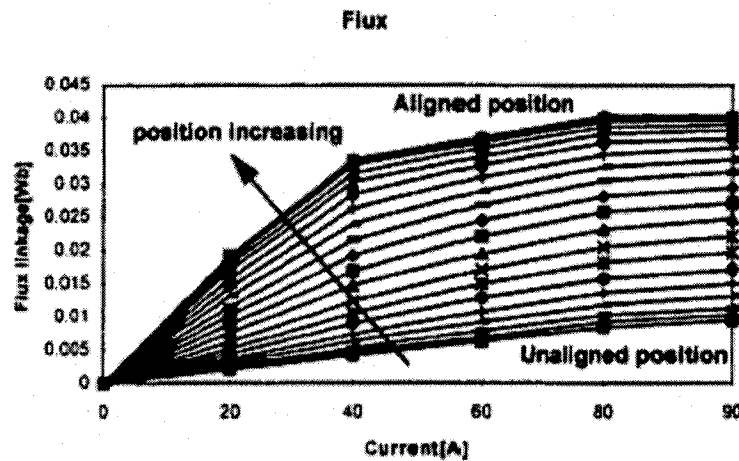


Figure 2.1: Flux-linkage as a function of stator phase current and rotor position.

Local and bulk saturation are two types of saturation that are to be considered. Local saturation occurs when the poles are just approaching or just leaving the overlapping position. This leads to tip saturation because of flux fringing. Bulk saturation occurs in fully aligned position resulting in a huge loss of torque produced by the machine [23].

From figure 2.1, it should also be noted that there are two types of non-linearity present in the flux-linkage characteristics. First, the variation of flux-linkage with current at any given rotor position is non-linear due to magnetic saturation. Second, the flux lines are not displaced equally with respect to each other. As shown in figure 2.1, the flux-linkage lines are drawn for different currents with equal increments of rotor angle from unaligned position to aligned position. The iso-flux-linkage lines are crowded near the unaligned and aligned rotor position and they are less crowded at the middle. Therefore, it is difficult to analytically express the static characteristics [23].

Thus, the electromagnetic behavior of the SRM can be represented by its static characteristics, either by plotting the inductance variation or the flux-linkage variation with rotor position and stator phase current.

2.1.2 Torque Production Mechanism in SRM Drives

Figure 2.2 shows the flux-linkage versus current for a given rotor position. For a phase coil with current i_k linking with a flux Ψ_k , the stored field energy W_f and the coenergy W' are indicated as shaded regions. Co-energy can be found from the definite integral [24],

$$W' = \int_0^1 \Psi_k di$$

The torque produced by one phase coil at any rotor position is given by,

$$T = [\partial W' / \partial \Phi]_{i=\text{constant}}$$

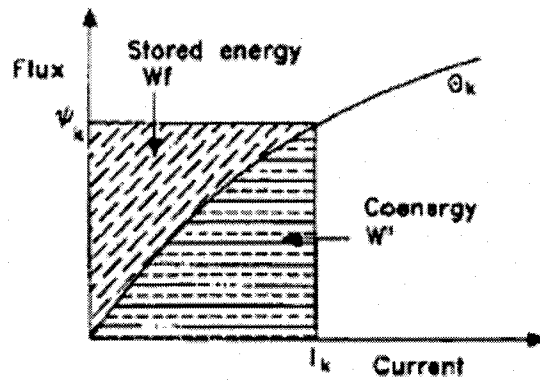


Figure 2.2: Stored field energy and coenergy

In the absence of magnetic saturation, the magnetization curve in figure 2.2 would be a straight line and the coenergy would be equal to the stored field energy. The instantaneous torque then reduces to

$$T = \frac{1}{2} i^2 \frac{dL}{d\Phi}$$

Positive (motoring) torque is produced by phase current flow in the rising inductance region, while placing the current pulses in the falling inductance region produces negative (generating) torque. The above equation suggests that the sign of the torque is independent of the direction of the current flow in the phase winding. Thus, in order to produce positive unidirectional torque, each phase should be energized during the rising inductance region. By sequentially exciting the phases, the total torque will be unidirectional. This clearly shows the necessity for an external position sensor [24].

2.1.3 SRM Chopper Topologies

The magnetic behavior of the SRM and the torque production mechanism were explained in the two previous sections. It was mentioned that the torque developed by the motor can be controlled by varying the amplitude and the timing of the current pulses in synchronism with the rotor position. The input to the SRM drive is dc voltage, which is derived from the Fuel Cell stack in this research. In certain applications it could be derived from the utility through a front-end diode rectifier or batteries. The currents in SRM are unidirectional and the chopper configuration should suit this requirement.

In literature, several chopper topologies for SRM drives have been proposed [26]-[28] and the most commonly used chopper uses two-switches and two freewheeling diodes per phase and is called classic chopper, which is shown in the following figure.

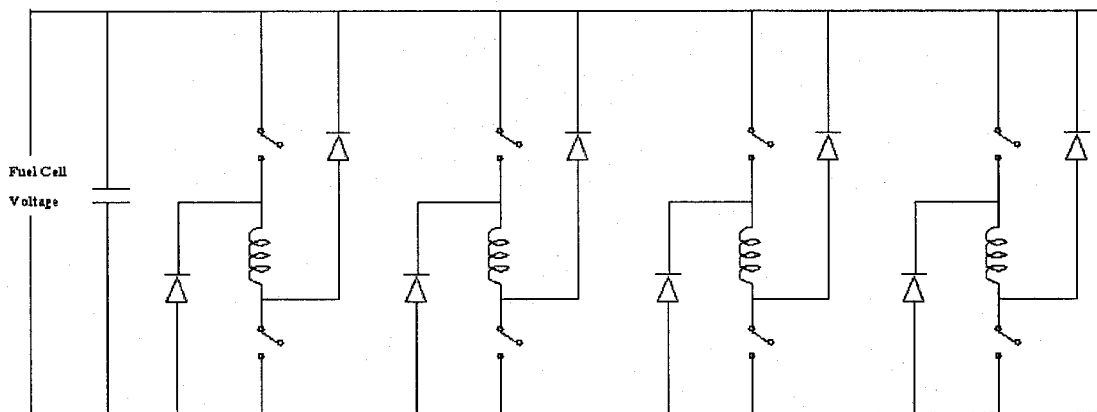


Figure 2.3: SRM Classic Chopper

The main advantage of using a classic chopper is the flexibility in control. All the phases can be controlled independently which is very essential for very high speed operation, where there will be considerable overlap between the adjacent phase currents.

In the classic chopper, both the controlled switches are turned on simultaneously so that the motor winding will be connected to the dc bus voltage. Both the switches are turned off simultaneously when it is desired to turn off the phase, figure 2.4 shows the modes of operation for one phase of the SRM chopper. The phase current flows through the freewheeling diodes and returns the trapped magnetic energy into the dc link. During freewheeling, the motor phase is subjected to negative of the bus voltage through the freewheeling diodes. In order to provide current feedback to the controller, a current sensor can be connected in series with the phase winding [24].

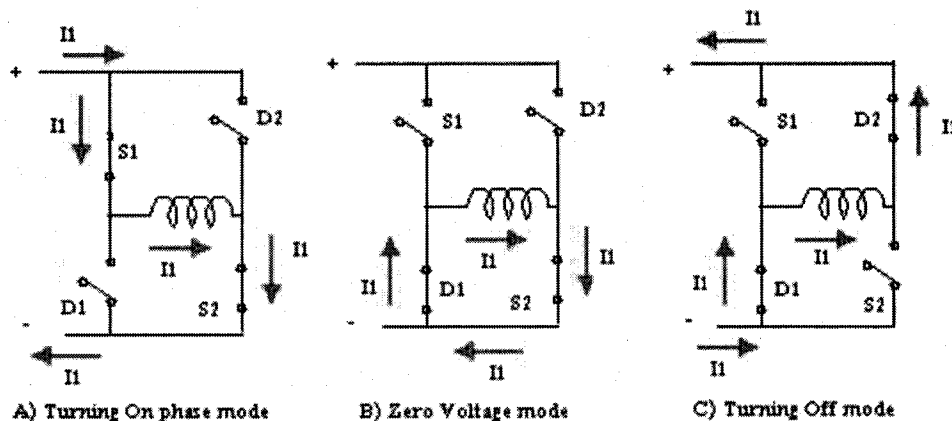


Figure 2.4: Modes of operation for one phase of the SRM chopper

The choppers used for SRM drives usually employ IGBTs or power MOSFETs depending on the operating voltage levels. In certain automotive applications, the voltage level is limited and hence the SR motors are designed to be of low-voltage, high current type. For such applications, MOSFETs are employed. For home appliance applications, the voltage level corresponds to the main supply and hence IGBTs are ideally suited for the chopper. The freewheeling diodes used in the choppers should be ultra high-speed type and typically Schottky diodes are used. The chopper also has an input filter, which can supply the demanded ripple current. The SRM converter that is used for this research is the Classic Converter using MOSFETs as switches [25], which is shown in the following figure.

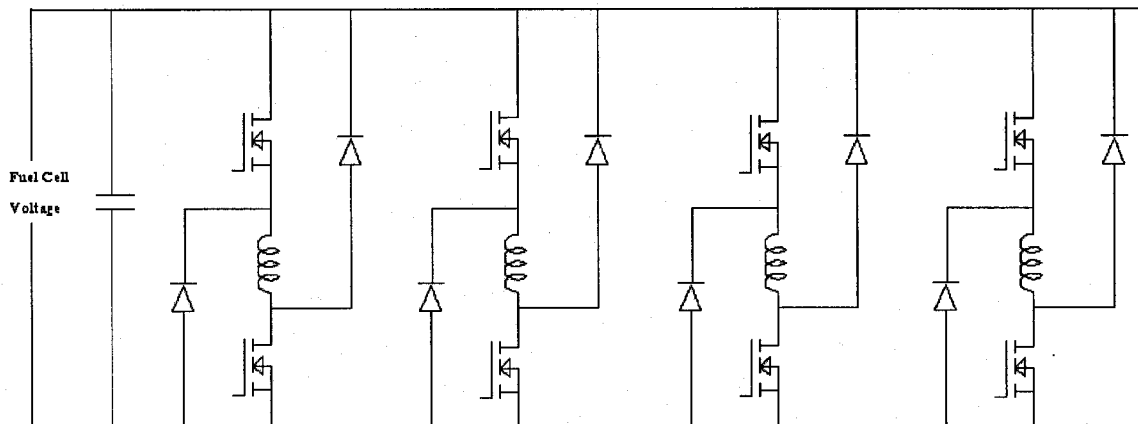


Figure 2.5: SRM Classic Chopper using Power MOSFETs

Figure 2.6 shows one of the other types of the choppers that are used with SRM in other applications. This chopper is known as C-dump chopper, which is employing single-switch per phase in which the magnetic energy during freewheeling is dumped into a capacitor, which in turn is returned to the dc source [26]-[28].

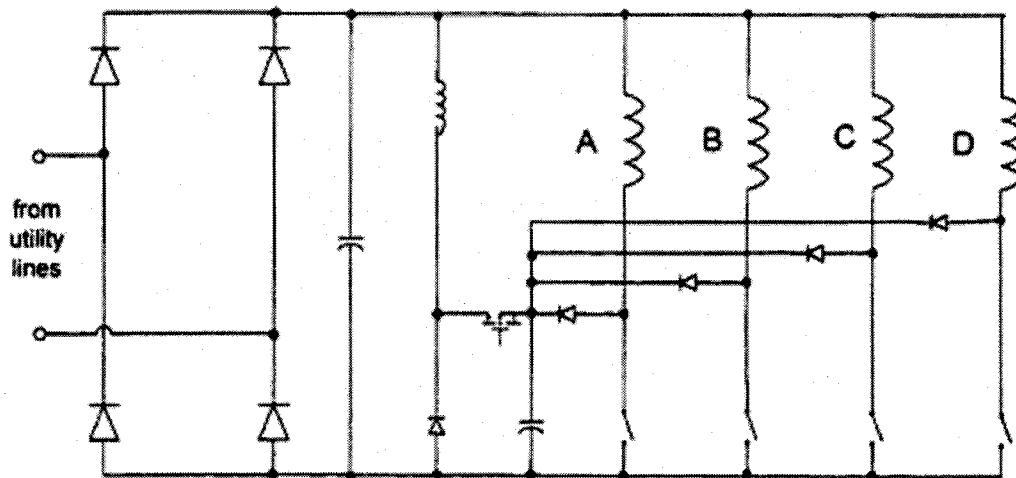


Figure 2.6: C-dump chopper

A chopper circuit is used to transfer the energy in the capacitor to the dc supply. Though the circuit is highly efficient, it requires additional components with accurate control of the chopping circuit for efficient energy recovery. There are three more types of choppers that were used with SRM in different applications in literatures, which are shown in the following figure.

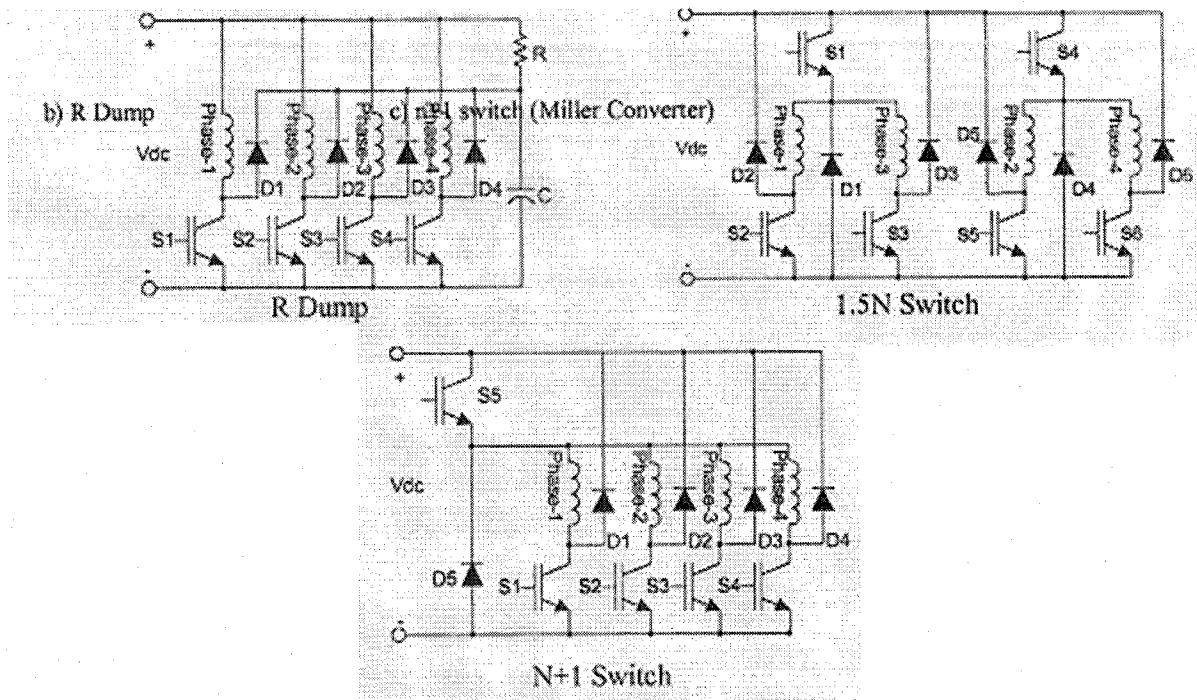


Figure 2.7: Three Different Types of SRM Chopper

The poor power factor is one of the main problems associated with SRM drives compared to the other motors like BLDC and induction motors. This is mainly because, the trapped energy is returned to the dc bus during the freewheeling action. Moreover, the magnetizing component of the current in an SRM is drawn from the dc bus itself unlike permanent magnet machines, where the flux component of the armature current is negligibly small. Therefore, the KVA rating of the inverter for an SRM drive is very high compared to that of BLDC and induction motor drives [25].

2.1.4 Theory of The SRM Inductance Model

The SRM model that was used for this research is an inductance model that was previously designed in [23]-[25] (Author Dr. M. Ehsani). The idea of using this design model for SRM other than other design models came from the simplicity of the model and its ability to run in real time with the drive controller that is designed in this research and the Fuel Cell stack model.

In the previous sections, the magnetic behavior of the SR motor and also the torque production mechanism were reviewed. From the mechanism of torque production, it is evident that the excitation of the stator phases needs to be synchronized with rotor position in order to produce unidirectional torque. In a switched reluctance motor, each active phase is represented by a first order non-linear differential equation which has inductance term in it as shown in the following equation [23]-[25].

$$v_j = R i_j + \sum_{k=1}^m \left\{ i_k \frac{\partial L_{kj}(\theta, i)}{\partial i_k} \frac{di_k}{dt} + L_{kj}(\theta, i) \frac{di_k}{dt} + i_k \frac{\partial L_{kj}(\theta, i)}{\partial \theta} \omega \right\}$$

Moreover, the phase inductance varies with rotor position and instantaneous phase current and the nature of variation is highly non-linear. In the following voltage equation, the active phase voltage and current are measurable and the phase resistance is a constant parameter neglecting the temperature effects [23]-[25].

$$v_j = R i_j + \sum_{k=1}^m \frac{d\psi_{kj}(\theta, i)}{dt}$$

In the following sections, the variation of the stator phase inductance with rotor position and instantaneous phase current is expressed analytically. This inductance expression is used in the voltage representing the active phase of the motor and the voltage equation is solved to estimate the rotor position indirectly. In the remaining sections of this chapter, the dynamic equations of the active phase are presented first, followed by the inductance model developed.

A. Dynamic Equations of The SRM Drive

A first order non-linear equation is used to describe each active phase in the SRM. Kirchhoff's voltage law was applied to the active phase to obtain the above voltage equation.

Hence the voltage equation of one of the active phases is given by,

$$v_j = R i_j + \sum_{k=1}^m \frac{d\psi_{kj}(\theta, i)}{dt} \quad (2.1)$$

where, v_j is the active phase voltage in volts, R is the phase resistance in Ohms, i_j is the phase current in Amps, ψ_{kj} is the total flux-linkage of the active phase in Wb-turns, 'm' is the number of phases.

Both self and mutual flux-linkages are included in the flux-linkage in the active phase. The mutual fluxes in the SRM is a small percentage of the total flux and can be neglected [29] and hence (2.1) can be simplified to the following:

$$v = Ri + \frac{d\psi(\theta, i)}{dt} \quad (2.2)$$

The subscripts in the voltage equation are dropped for the sake of simplicity.

The product of the self-inductance and the instantaneous phase current gives the flux-linkage of the active phase.

$$\psi(\theta, i) = L(\theta, i)i \quad (2.3)$$

where, $L(\theta, i)$ is the self-inductance of the active phase in H.

Substituting (2.3) into (2.2) gives,

$$v = Ri + L(\theta, i)\frac{di}{dt} + i\frac{dL(\theta, i)}{d\theta}\frac{d\theta}{dt} + i\frac{dL(\theta, i)}{di}\frac{di}{dt} \quad (2.4)$$

Or equivalently,

$$v = Ri + L(\theta, i)\frac{di}{dt} + i\omega\frac{dL(\theta, i)}{d\theta} + i\frac{dL(\theta, i)}{di}\frac{di}{dt} \quad (2.5)$$

where, ω is the angular speed of the rotor, in radians/second.

In (2.4), the first term in the right hand side is the resistance drop and the second term is the self-inductance drop. The third term corresponds to the voltage drop due to the speed induced emf and the final term is the incremental inductance drop term.

The active phase quantities in (2.5) are measurable, and equation (2.5) can be solved to get the rotor position, if the inductance variation with rotor position and the stator phase current can be expressed analytically. The details of the SRM inductance model used in this research along with the procedure of deriving the model will be described in the next section.

B. Derivation of The SRM Inductance Model

The phase inductance in the SRM is a periodic function of the rotor position. Because of the magnetic saturation, the phase inductance varies with instantaneous phase current at any given position. Several different ways have been developed to model the static characteristics of the SRM, either variation of the flux-linkage or the phase inductance with rotor position considering magnetic saturation [29]. Some of these ways use look up tables based on experimental results, and some of them use analytical models to describe the inductance function.

To model the SRM inductance model, the static characteristics of the SRM are represented by inductance model rather than flux-linkage model. A 90KW, 25,000 RPM, 8/6, 4-phase SRM is used to design the inductance model. The geometry details of the motor that was used in [23]-[25] to develop the inductance model are presented in Appendix A.

The phase inductance can be represented using the following expression:

$$L(\theta) = \sum_{n=0}^m L_n \cos(nN_r \theta + \phi_n) \quad (2.6)$$

where 'Nr' is the number of rotor poles, 'm' is the order of approximation, ' ϕ_n ' is the phase angle of the n^{th} harmonic with respect to the fundamental.

Because of magnetic saturation, the inductance depends on the instantaneous phase current. The coefficients of the Fourier series are expressed as functions of the instantaneous phase current, in order to represent the dependence of phase inductance on the phase current, which results in the following:

$$L(\theta, i) = \sum_{n=0}^{\infty} L_n(i) \cos(nN_r\theta + \phi_n) \quad (2.7)$$

The above equation is expanded into the following:

$$L(\theta, i) = L_0(i) + L_1(i)\cos(N_r\theta + \phi_1) + L_2(i)\cos(2N_r\theta + \phi_2) + \dots \quad (2.8)$$

At $\theta = 0$, L is maximum and at $\theta = (\pi/N_r)$, L is minimum when a cosine function is used. It can be shown that $\phi_n=0$, for $n=0,1,2,\dots,m$, by substituting these conditions in (2.8). In this research a four phase motor is used for the simulation. From [23]-[25] experimentally measured unsaturated inductance data, it has been found that considering only the first three terms of the Fourier series results in a good approximation for the inductance. Therefore equation (2.8) gets simplified to the following:

$$L(\theta, i) = L_0(i) + L_1(i)\cos(N_r\theta) + L_2(i)\cos(2N_r\theta) \quad (2.9)$$

The following step is to identify a function for the Fourier Coefficients $L_0(i)$, $L_1(i)$, $L_2(i)$ in terms of the stator phase current that will take care of the effect of magnetic saturation on the inductance. There are two kinds of saturation in SRM, as mentioned earlier. The first saturation is called bulk saturation that occurs at the aligned position. The second saturation is called local saturation that occurs at discrete rotor positions, when the rotor poles just approach the stator poles and just begin to move towards the aligned position.

The aim of [23]-[25] work is to arrive at a model that very closely matches the inductance characteristics while requiring minimum amount of finite element data, which will give a useful SRM model for any other future work or research using SRM like this research.

The first step [23]-[25] started with is a two-dimensional finite element model of the experimental motor is built in Maxwell package [30]. From the data obtained through finite element analysis, it has been found that expressing the inductance at the aligned position as a polynomial function of the phase current results in good accuracy. The variation of the aligned phase inductance with current as obtained through finite element analysis [23]-[25] is shown in the following figure.

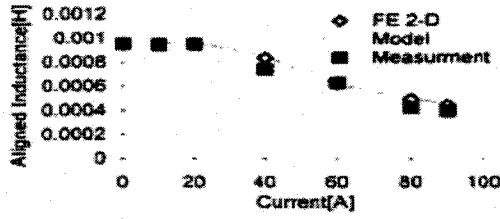


Figure 2.8: Variation of inductance at the aligned position with current

The order of the polynomial function is limited to 5. Thus, the stator phase inductance at the aligned position can be expressed as,

$$L_a(i) = L(\theta = 0^\circ) = \sum_{n=0}^{n=k} a_n i^n \quad (2.10)$$

Because of the large air gap in the flux path, the phase inductance at the unaligned position can be assumed to be a constant and is given by,

$$L_u = L(\theta = \frac{\pi}{N_r}) \quad (2.11)$$

Moreover, the phase inductance at the unaligned position is assumed constant, because the phase current does not influence it. A point midway between the aligned and unaligned position is chosen for analysis. In order to obtain numerical data, the finite element model of the motor is modified to correspond to a rotor position midway between the aligned and unaligned position, which is expressed as,

$$L_m(i) = L(\theta = \frac{\pi}{2N_r}) = \sum_{n=0}^{n=k} b_n i^n \quad (2.12)$$

The Fourier coefficients in (2.8) need to be defined in terms of $L_a(i)$, L_u , and $L_m(i)$ as given by equations (3.10)-(3.12) respectively. The coefficients $L_0(i)$, $L_1(i)$, $L_2(i)$ are related to the inductance terms $L_a(i)$, L_u and $L_m(i)$ using the following boundary conditions:

At $\theta = 0$, which corresponds to the aligned position,

$$L(0,i) = L_a(i) + L_1(i) + L_2(i) = L_a(i) \quad (2.13)$$

At $\theta = \pi$, which corresponds to the unaligned position,

$$L(\pi,i) = L_a(i) - L_1(i) + L_2(i) = L_u \quad (2.14)$$

At $\theta = \pi/2$, which corresponds to the midway point between the aligned and unaligned position,

$$L_m(i) = L(\theta = \frac{\pi}{2N_r}) = \sum_{n=0}^{n=k} b_n i^n \quad (2.15)$$

Substituting equations (2.10)-(2.12) in equations (2.13)-(2.15), the following relations are derived:

$$L_0(i) = \frac{1}{2} \left[\frac{1}{2} (L_a(i) + L_u) + L_m(i) \right] \quad (2.16)$$

$$L_1(i) = \frac{1}{2} (L_a(i) - L_u) \quad (2.17)$$

$$L_2(i) = \frac{1}{2} \left[\frac{1}{2} (L_a(i) + L_u) - L_m(i) \right] \quad (2.18)$$

Thus, the inductance model is derived by obtaining the finite element analysis data at three different rotor positions [23]-[25]. The order of the polynomial function is limited to 5, and the numerical values of the polynomial coefficients obtained are shown in appendix A. By this, the development of the SRM model for the phase inductance is complete.

2.2 Fuel Cell Stack Model

The ever increasing need for electrical power generation, rapid progress in power deregulation, and the environmental concerns over the use of fossil fuels for electric power generation have attracted much attention to fuel cell power generation system. Therefore, the idea of using fuel cell stack as a power generation for SRM in this research is based on the fact that the fuel cell as a power generation system has low pollution, high efficiency, and diversity of fuels, reusability of exhaust heat and many other advantages [31].

A fuel Cell is an electrochemical device that produces direct current electricity through the reaction of hydrogen and oxygen in the presence of an

electrolyte. The fuel cell generation system consists of a reformer, a stack and power converter as shown in figure 2.9, for the purpose of this research only the stack and the power converter are designed and implemented. The reformer produces hydrogen gas from fuel and then supplies it to the stack. The stack is a collection of unit cells, and the unit cells consist of electrolyte, separators, and plates. The output of the fuel cell is a result of a chemical reaction and possesses nonlinear characteristics [31].

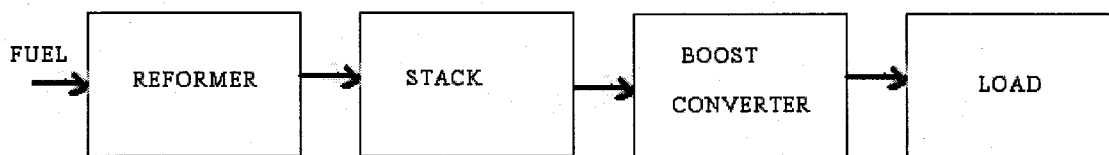


Figure 2.9: Fuel Cell System

On the other hand the power converter converts low voltage dc to ac or high voltage dc. The power converter must have functions to protect the system from output fluctuations reverse currents, and sudden load variations to assure their full lifetime, therefore for the purpose of this project a PID controller is designed for the dc/dc power converter. Also the performance of the fuel cell generation system is very sensitive to the load variations, since it has low voltage and high current output characteristics [32].

Fuel cell has two electrodes, a positive electrode and a negative electrode, which are separated by an electrolyte. A hydrogen-rich fuel passes through an electrochemical fuel processor (reformer), where hydrogen is produced and fed to the anode, and an oxidant is fed continuously to the cathode. Since, the Fuel Cell power generation system that modeled in Simulink for this project is only the fuel cell stack, direct hydrogen is used as the input for the stack [32].

The existence of excess charge at the electrodes brings about a potential difference between them. When an electric load is connected between the two electrodes, positive or negative ions flow through the electrolyte, hence producing an electric current. Heat, clean water, and oxidant(s) are the byproducts of this electrochemical process [32].

A single Fuel Cell element generates high current, low voltage DC electricity. Therefore, fuel cells are grouped in series, called a “stack”, in order to obtain a sufficient voltage and power output. In addition to that, fuel cells do not store energy in the cells and run down when the stored energy is released, like batteries. They produce electricity as long as hydrogen-rich fuel (Ex. Natural gas, Methanol, landfill gas and coal-derived gas) is available to them. Since the aim of this research is the drive control for the SRM, the following sections will be briefly describing the System interactions for the Fuel Cell and each system corresponding control objective. Moreover, Emmeskay’s Fuel Cell Stack simulink model that is used in this research as the power source will be briefly explained.

2.2.1 System Interactions

For the viability, efficiency, and robustness of fuel cell propulsion systems, precise control of the reactant flow and pressure, stack temperature, and membrane humidity will be critical. The over all fuel cell stack system could be partitioned into four subsystems. Each system has a corresponding control objective and also interactions with other subsystems. The subsystems are the

reactant flow, the heat and temperature, the water management, and the power management subsystems [33].

A. Reactant Flow Subsystem

The reactant flow subsystem consists of hydrogen supply and air supply loops. When the vehicle traction motor draws current, hydrogen and oxygen become depleted in the fuel cell stack. The valve and compressor motor are used to adjust the hydrogen flow in the anode and the air flow in the cathode respectively. The control objective is to provide sufficient reactant flows (to keep the desired excess ratio) to ensure fast transient response and to minimize auxiliary power consumption [33].

B. Heat and Temperature Subsystem

The heat and temperature subsystem includes the fuel cell stack cooling system and the reactant temperature system. Heat is generated in the fuel cell as the traction motor draws current. First, de-ionized water is used as coolant in the stack instead of an effective coolant fluid. Second, the PEM fuel cell is designed to operate at the temperature around 80°C. Hence, the exhaust air exiting the stack, which has temperature around 80°C, has less ability to carry out heat than the ICE exhaust gas, which is over 500°C. The cooling system is responsible for the heat rejection for the fuel cell stack. The low temperature difference between the stack and the water coolant limits the effectiveness of the heat transfer from the stack to the coolant. Therefore, active cooling is required

through the reactant flow rate and the cooling system. Furthermore, the temperature of inlet reactant air also affects the temperature of the stack. The heat management system can vary the speed of the cooling fan and the recirculation pump in coordination with adjusting a by-pass valve. Fast warm-up with no stack temperature overshoot and low auxiliary fan and pump power is the goal of thermal management [33], [34].

C. Water Management Subsystem

The use of the water management system is to maintain hydration of the polymer membrane and to balance water usage/consumption in the system. The humidity of the membrane is affected by the amount of reactant flow and the water injected into the anode and cathode flow streams. Water molecules are both produced in the cathode and dragged from the anode to the cathode by the hydrogen protons, as the current is drawn from the fuel cell. The concentration gradient causes water to diffuse from the cathode to the anode, as the concentration of water in the cathode increases. Different mechanisms such as water generated while load increases, changes in the absolute and relative reactant pressure across the membrane, changes in air flow rate, and changes in stack temperature can cause perturbation in fuel cell humidity. These mechanisms indicate strong and nonlinear interactions among the humidity control. If there is no proper humidification control a 20-40% drop in fuel cell voltage could occur [33], [34].

D. Power Management Subsystem

The power drawn from the fuel cell stack is controlled by the power management subsystem. Without considering power management, the load current can be viewed as a disturbance to the fuel cell system. However, if a battery is used as another power source in the system, the power management between two power sources could be applied with the objective of giving a satisfactory vehicle transient response and assisting the fuel cell system [33], [34].

E. Fuel Processor Subsystem

Fuel processor technology is an important part of the fuel cell system due to the inadequate infrastructure for hydrogen refueling, distribution, and storage. Methanol, gasoline, and natural gas are examples of fuels being considered as fuel cell energy sources. Different processes involved in converting carbon-based fuel to hydrogen are shown in figure 2.10. The fuel processor variables that require precise control include the temperature of the reactors and the concentration of hydrogen and carbon monoxide in the gas stream [33], [34]. For the purpose of this research, direct hydrogen process is used for the Fuel Cell stack simulink model that was developed by Emmeskay Inc.

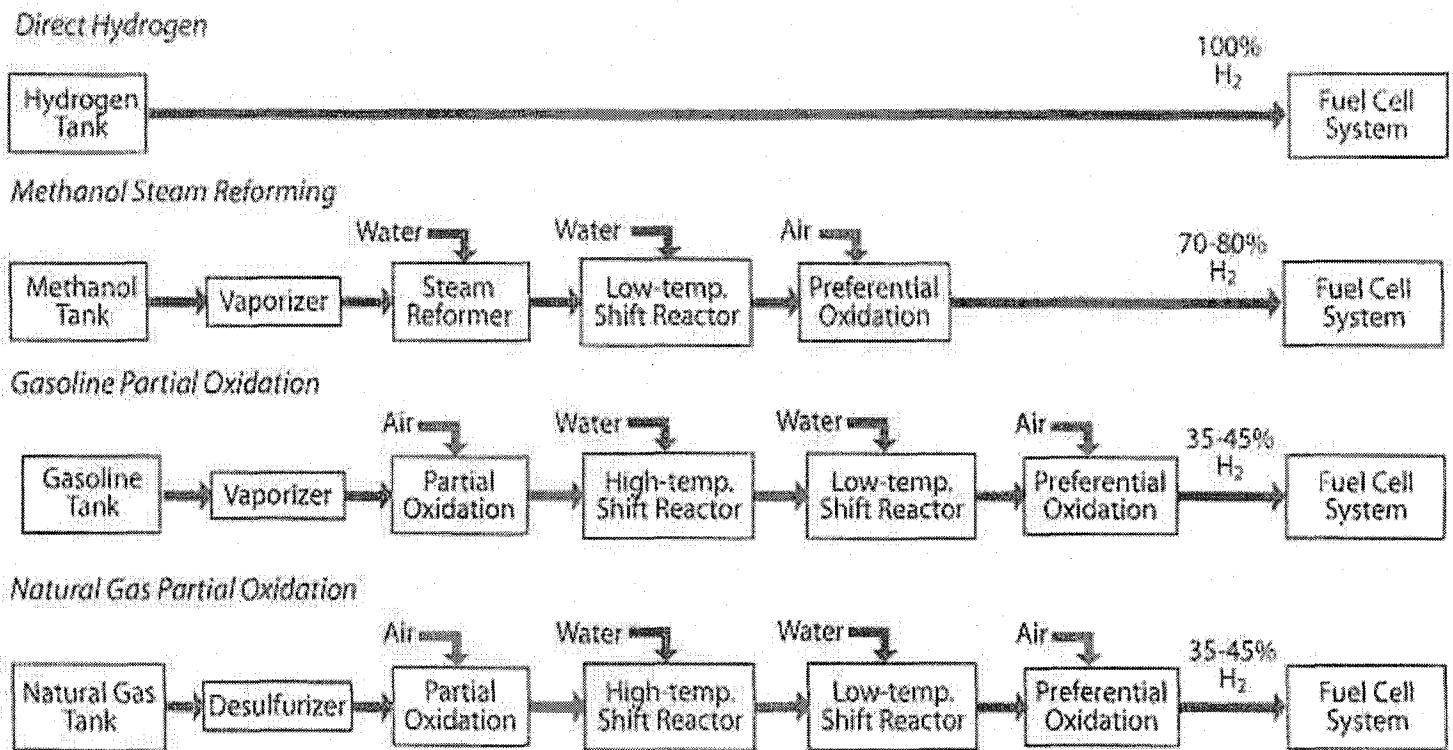


Figure 2.10: Fuel Sources for Fuel Cell Systems

2.2.2 Fuel Cell Stack Model

The above sections gave a brief introduction for the Fuel Cell process and its different subsystems and their relative control parameters. This section will explain briefly the Fuel Cell stack simulink model used in this research.

The model consists of seven blocks, fuel cell stack, coolant controller, fuel cell controller, anode pressure, anode valve, cathode pressure, and cathode valve. The fuel cell stack block has 13 inputs and 5 outputs. The temperature values for each of the cathode, anode, coolant and ambient are set to a constant value for each one of them. Also constant values were set for each of the amounts of N_2 , H_2 , O_2 , H_2O , CO_2 at the cathode and the anode. On the other

hand, the coolant controller used the cathode output temperature from the fuel cell stack and the cathode set point temperature as its inputs to output the coolant amount to be used as input for the fuel cell stack.

The anode and cathode pressure blocks and valve blocks act as a pressure controller for each of the anode and the cathode. They use the output for the anode and cathode pressures from the fuel cell stack, and they input the anode and cathode pressures that are used as inputs back to the fuel cell stack. While the Fuel Cell controller uses the fuel cell voltage and current to output the fuel cell power.

The main output for the fuel cell is the fuel cell voltage and power, which are used as the inputs for the load. In this research only the fuel cell voltage was used as input for the load (SRM). A dc/dc boost converter is used to boost up the fuel cell voltage to the required voltage (from 150v to 270v) to drive the SRM.

Moreover, the load current is used as input for the fuel cell stack to help controlling the fuel cell stack current. Since the SRM has four phases, therefore it produces four currents, and the Fuel cell stack can only accept one load current. Therefore, current converter is used to convert the SRM four currents to one load current that will be fed back to the fuel cell stack. This was a brief description for Emmeskay Inc. Fuel Cell Stack Model that is used in this research as the power supply for SRM. The fuel cell stack simulink model is shown in appendix A.

CHAPTER 3

SRM DRIVE CONTROLLER

The last two chapters gave a brief introduction for the Switched Reluctance Motor and the Fuel Cell. This chapter will be describing the first main goal for this research, which is designing a drive controller for switched reluctance motor to have a constant speed and a smooth torque for the motor. The drive controller consists of a hysteresis current controller, commutation angle controller and a PI Speed controller. The design method that is used to design the commutation angle controller is the sensorless control method, because it requires minimum amount of hardware while giving position information continuously with good accuracy. It also utilizes only the active phase voltage and current measurements thereby eliminating the external rotor position sensor and also additional electronics.

The sensorless control method was applied for designing the commutation angle controller which outputs the commutation angle that is fed to the hysteresis current controller to energize the active phase of the SRM drive, to stabilize the SRM phase currents and to smooth the motor torque knowing the rotor position information. While the PI Speed controller is designed to obtain a constant speed for the SRM at different loads.

Several sensorless control techniques have been developed over the past few years, which use d-q transform equations [35] in the case of vector controlled induction motor drives. It is possible to encode the rotor angle through real-time

computation, by measuring the terminal voltages and currents. In the case of Switched Reluctance Motors, there is a definite advantage. For achieving sensorless control, the stator phase inductances, which vary periodically with rotor position, can be utilized. Therefore it is possible to sense the rotor position electronically and eliminate external position sensors.

Increased reliability, reduced cost and drive dimension, and no need for additional cabling are some of the advantages of sensorless control in electrical machines. Ideally the sensorless control algorithm should be simple and easily implementable. It should also be capable of providing rotor position information continuously with high resolution and accuracy over the desired operating speed range.

Several patents and research papers have been published in the last decade on sensorless control of SRM drives [36] – [59]. Almost all the methods utilize the fact that the stator phase inductance in an SRM varies periodically with rotor position. The expanded voltage equation of an active phase in an SRM in a generalized form, which was presented in chapter 2, is given as follows:

$$v_j = Ri_j + \sum_{k=1}^m \left\{ i_k \frac{\partial L_{kj}(\theta, i)}{\partial i_k} \frac{di_k}{dt} + L_{kj}(\theta, i) \frac{di_k}{dt} + i_k \frac{\partial L_{kj}(\theta, i)}{\partial \theta} \omega \right\}$$

The first term in the right hand side of the above equation is the resistive drop and doesn't offer position information. The remaining three terms in the right hand side have inductance terms in them and therefore they have rotor position information. Thus it is possible to obtain rotor position information indirectly from one of these terms of the active phase voltage equation.

3.1 Formulation of The Sensorless Algorithm

Chapter 2 described the derivation of the inductance model and also presented the voltage equations of the active phase in the Switched Reluctance Motor. This chapter will explain the formulation of the sensorless control algorithm from these equations. As described in Chapter 2, the voltage equation of the active phase is given by,

$$v = Ri + \frac{d\psi(\theta,i)}{dt} \quad (3.1)$$

where, v is the voltage applied across the winding in V, ' R ' is the phase resistance in Ω , $\psi = L(\theta,i)*i$, is the flux linkage in wb-turns, $L(\theta,i)$ is the self-inductance of the phase in H, i , is the phase current in A. Equation (3.1) can be expanded as follows,

$$v = Ri + L(\theta,i) \frac{di}{dt} + i\omega \frac{dL(\theta,i)}{d\theta} + i \frac{dL(\theta,i)}{di} \frac{di}{dt} \quad (3.2)$$

In equation (3.2) the last term in the right hand side is negligibly small compared to the other terms. By substituting the analytical expression used to describe the phase inductance, which is described in chapter 4 into (3.2), the rotor position information can be obtained. The formulation of the sensorless control algorithm depends on the operating speed range of the motor. The formulation of the sensorless control algorithm for low and high speed operating points will be described separately in the following subsections.

3.1.1 Low Speed Operation

The angular speed is zero at standstill and therefore the third term in (3.2) vanishes. The angular speed will be very small and hence the third term in the right hand side of (3.2) as compared to the other two terms can be neglected, when the rotor speed is very low, say a few tens of revolutions per minute. Therefore, (3.2) simplifies to the following:

$$v = Ri + L(\theta, i) \frac{di}{dt} \quad (3.3)$$

In the above equation, the active phase voltage and current are measurables and the resistance can be assumed to be a constant. Thus (3.3) can be rearranged to the following:

$$L(\theta, i) = \frac{v - Ri}{(di/dt)} \quad (3.4)$$

The rotor position can now be estimated using the inverse function of the inductance term in (3.4) and is given by,

$$\theta = L^{-1} \left[\frac{v - Ri}{(di/dt)} \right] \quad (3.5)$$

3.1.2 High Speed Operation

The third term in (3.2), which represents the speed-induced emf, will no longer be small compared to the other two terms, when the rotor speed increases beyond a certain value. Thus, (3.1) can be directly used for position estimation. Integrating (3.1) with respect to time and rearranging the terms we get,

$$L(\theta, i) = \frac{\int (v - Ri) dt}{i} \quad (3.6)$$

Like the low speed case, the rotor position can now be estimated using the inverse function to the inductance term in (3.4) and is given by,

$$\theta = L^{-1} \left[\frac{\int (v - Ri) dt}{i} \right] \quad (3.7)$$

Equations (3.5) and (3.7) suggest that it is possible to estimate the rotor angle once the active phase voltage and current are available. Therefore, by using the inductance model presented in chapter 2, the rotor position can be estimated in real-time through active phase voltage and current measurements.

3.2 Commutation Angle Controller

The current waveform should be shaped properly, to maintain the desired torque at different loads. Usually, there are two major factors that influence the current waveform. One is firing angle; another is switching method. The firing angle will be controlled with the commutation angle controller, while the switching method will be done with the hysteresis current controller.

For the SRM, each phase current is always built up from zero. Each phase is excited between the unaligned and aligned position. The dwell angle is defined as $\theta_c - \theta_0$, where θ_0 is the starting angle and θ_c is the commutation angle. Usually, the firing angles θ_0 , θ_c are selected to avoid the phase current to be overlapped. Adjusting the firing angles θ_0 , θ_c according to the rotor speed can also shape the current waveform. Because the Electro Magnetic Force increases with the speed, the turn-on angle should be advanced to unaligned position, even into the previous zone of falling inductance when the rotor speed is high. As a result, the current can grow to the adequate level at a desired rate. So, the whole motor operation process can be divided into four modes in terms of the firing angles [60].

These four modes are:

- 1) normal mode at low speed;
- 2) boost mode at high speed;
- 3) an advanced mode at very high speed;
- 4) braking mode at the speed exceeding the reference speed. The following figure shows the firing angle varying with the rotor speed.

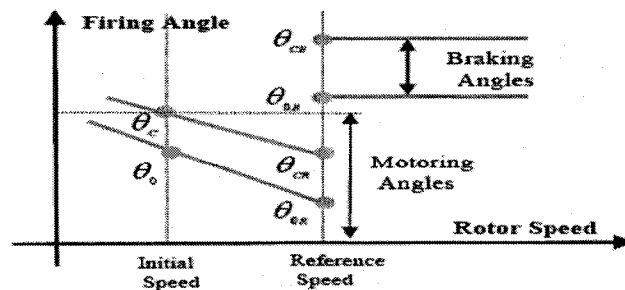


Figure 3.1: Firing angles vary with rotor speed

In the next chapter, the implementation of the Commutation angle controller and the simulation results will be presented.

3.3 Hysteresis Current Controller

A hysteresis current controller has been implemented in this research to generate the SRM chopper switching signals using the reference current produced from the PI-speed controller. Hysteresis current control is a method of controlling a voltage source chopper so that an output current is generated which follows a reference current waveform. This method controls the switches in the power chopper asynchronously to ramp the SRM current up and down so that it tracks a reference current signal.

A hysteresis current controller is implemented with a closed loop control system as shown in the following figure.

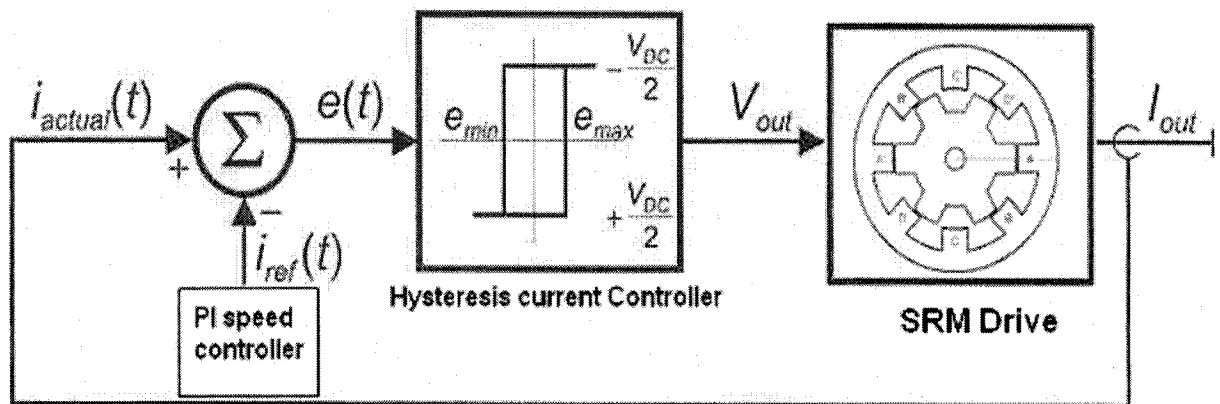


Figure 3.2: Hysteresis Current Controller block diagram

An error signal is used to control the switches in the power chopper. This error is the difference between the reference current, $i_{ref}(t)$, and the current being

produced from the SRM, $i_a(t)$. When the error reaches an upper limit, the MOSFETs are switched to force the current down. When the error reaches a lower limit the current is forced to increase.

The minimum and maximum values of the error signal are e_{\min} and e_{\max} respectively. The range of the error signal, $e_{\max} - e_{\min}$, directly controls the amount of ripple in the output current from the chopper and this is called the Hysteresis Band. The hysteresis limits, e_{\min} and e_{\max} , relate directly to an offset from the reference signal and are referred to as the Lower Hysteresis Limit and the Upper Hysteresis Limit. Even while the reference current is changing, the current is forced to stay within these limits. The following figure illustrates the ramping of the current between the two limits.

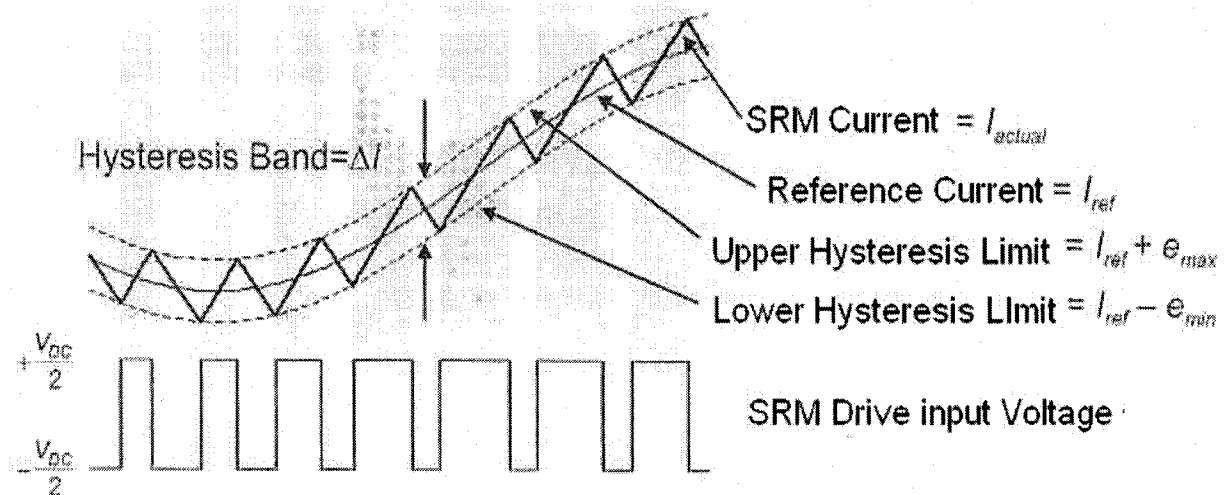


Figure 3.3: Operational Waveform

3.3.1 Hysteresis Current Controller Theory

Hysteresis current controller is a high frequency chopping current control, in which the main switches on each phase are switched on or off simultaneously with varying switching frequency to maintain constant current band. The hysteresis controller maintains the current waveform between an upper and a lower limit in the hysteresis band. The actual current is fed back to be compared with the reference current. Whenever the actual current exceeds the upper band, the output voltage changes from V to 0 and the current starts to decay. As soon as the current crosses the lower band limit the voltage changes back again and the actual current starts to increase.

Using the inductance based modeling equations for the SRM model developed in section (2.1.4), a vector of trigonometric elements and a vector consisting inductance profiles versus current at aligned, midway and unaligned positions [61] is given in the following,

$$\mathbf{L}(\mathbf{i}, \theta) = \mathbf{\Omega}^T(\theta) \mathbf{\Lambda}(\mathbf{i}) \quad (3.8)$$

where,

$$\mathbf{\Omega}(\theta) = \begin{bmatrix} 0.25 + 0.5 \cos(2N_p \theta) + 0.25 \cos(4N_p \theta) \\ 0.5 - 0.5 \cos(2N_p \theta) \\ 0.25 - 0.5 \cos(2N_p \theta) + 0.25 \cos(4N_p \theta) \end{bmatrix} \quad (3.9)$$

and $\mathbf{\Lambda}(\mathbf{i}) = [L_a(\mathbf{i}) \ L_m(\mathbf{i}) \ L_u(\mathbf{i})]^T$, such that $L_a(\mathbf{i})$, $L_m(\mathbf{i})$ and $L_u(\mathbf{i})$ are inductance profiles versus current at aligned, midway and unaligned positions, respectively. Using the phase voltage equation (3.2) and inductance in (3.8), the new voltage equation is obtained as

$$V_k = R_k i_k + \Omega^T(\theta) \left(i_k \frac{d\Lambda(\theta_k)}{d\theta_k} + \Lambda(\theta_k) \right) \frac{di_k}{dt} + i_k \Omega^T(\theta) \frac{d\Lambda^T(\theta)}{d\theta} \Lambda(\theta_k) \quad (3.10)$$

where, $k=1,2,3,4$ since it is a four phase motor. The coefficient of di/dt in the second term is incremental inductance, i.e.

$$L(i, \theta) = \frac{\partial L(i, \theta)}{\partial i} = \Omega^T(\theta) \left(i \frac{d\Lambda(i)}{di} + \Lambda(i) \right) \quad (3.11)$$

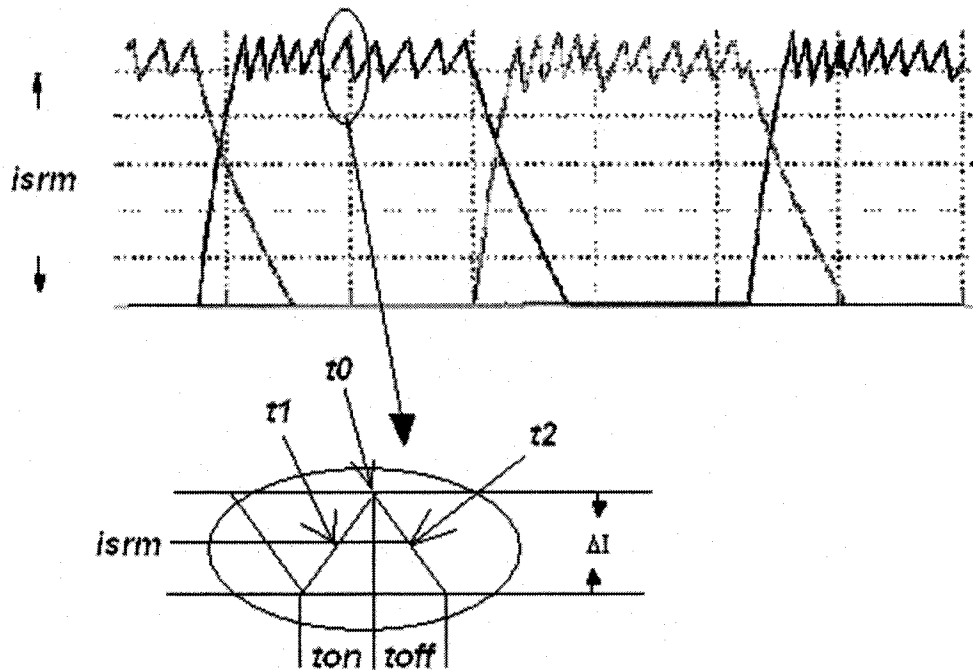


Figure 3.4: Ideal current waveform for deriving the hysteresis current controller equation

The above figure shows the chopping current waveform, where ΔI is the hysteresis band. Two specified consecutive time points in the rising and falling parts in that waveform and with the same level of current will be considered, i_{srm} as shown. Integrating the phase voltage equation in (3.3) between these two points will result in the following equation,

$$\int_{t_1}^{t_2} (V - ri) dt = \lambda(t_2) - \lambda(t_1) = \Delta\lambda \quad (3.12)$$

Since the flux linkage is a function of phase current and position, we can write

$$\Delta\lambda(i, \theta) = \frac{\partial\lambda}{\partial i} \Delta i + \frac{\partial\lambda}{\partial\theta} \Delta\theta \quad (3.13)$$

The first term in the above equation will be eliminated, because of the fact that the currents at those two points are the same. Consequently,

$$\Delta\lambda(i, \theta) = \frac{\partial\lambda}{\partial\theta} \Delta\theta = i \frac{\partial L(i, \theta)}{\partial\theta} \Delta\theta \quad (3.14)$$

Comparing the above equation with (3.13) and using (3.8) yields to

$$\int_{t_1}^{t_2} (V - ri) dt = i \frac{\partial L(i, \theta)}{\partial\theta} \Delta\theta = i \frac{\partial\Omega^T(\theta)}{\partial\theta} \Lambda(i) \Delta\theta. \quad (3.15)$$

Dividing both sides of the above equation by $\Delta t = t_2 - t_1$, the following equation is obtained.

$$H_c \Big|_{t_1, t_2} = \frac{\int_{t_1}^{t_2} (V - ri) dt}{t_2 - t_1} = i \omega \frac{\partial\Omega^T(\theta)}{\partial\theta} \Lambda(i). \quad (3.16)$$

Now, we expand the integral in the left-hand side of the above equation and assuming the phase voltage equal to $+V_{bus}$ and $-V_{bus}$ for the rising and falling periods, respectively. So we get

$$H_c = \frac{1}{t_2 - t_1} \left\{ V_{bus}(t_0 - t_1) - V_{bus}(t_2 - t_0) - r \left(i_c + \frac{\Delta i}{2} \right) \right\} \quad (3.17)$$

Defining a new parameter as γ , which is the ratio of the rising time to the falling time during a current chopping cycle, we get

$$\gamma = \frac{t_0 - t_1}{t_2 - t_0} \quad (3.18)$$

Finally, from (3.17) and (3.18), the hysteresis current controller estimation equation is obtained as

$$H_c = \left\{ \frac{\gamma-1}{\gamma+1} v_{bus} - r \left(i_c + \frac{\Delta I}{2} \right) \right\} \quad (3.19)$$

Now substituting hysteresis current controller from (3.17) and (3.18) in the phase voltage equation and solving that equation for incremental inductance, the position estimation equation, which is used in the commutation procedure, is obtained as

$$\ell(i, \theta) = \left\{ \frac{\gamma(\alpha-1) + (\alpha+1)}{\gamma+1} v_{bus} + r \left(i_c - i + \frac{\Delta I}{2} \right) \right\} \frac{1}{di/dt} \quad (3.20)$$

where

$$\alpha = \begin{cases} 1 & t_1 < t < t_0 \\ -1 & t_0 < t < t_2 \end{cases}$$

3.3.2 Commutation Procedure

The commutation strategy can be set by the designer or can be determined through a control system. In each case, this strategy determines $\theta_{k,off}$

and $\theta_{k+1,on}$, i.e., the angle at which the active phase is turned off and the angle at which the next phase is turned on. Then the corresponding incremental 'inductances' thresholds will be determined as following

$$\begin{aligned}\ell(i, \theta_{k,off}) &= \ell_{off}(i) \\ \ell(i, \theta_{k+1,on}) &= \ell_{on}(i)\end{aligned}$$

Comparing the right hand side of position estimation equation with these two thresholds does phase commutation. The following figure demonstrates a block diagram of the proposed method.

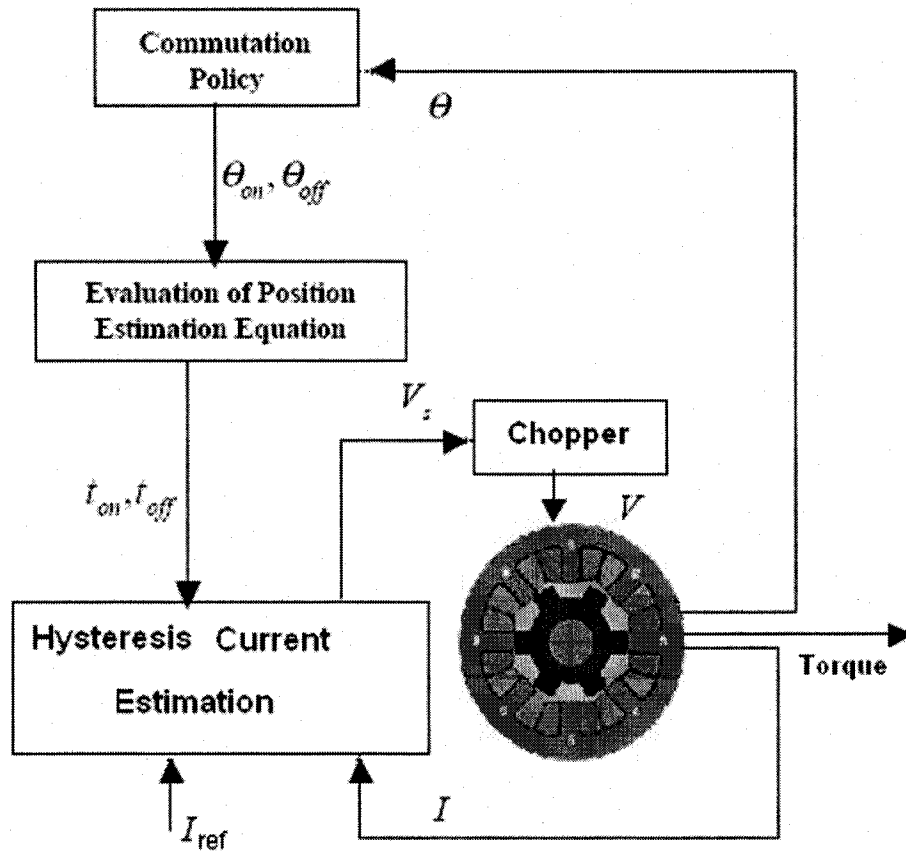


Figure 3.5: Block Diagram For The Current Controller Method

3.4 PI-Speed Controller

In this section, the design of a speed controller for the switched reluctance motor using Proportional-Integral control strategy is presented. While Proportional-Integral control represents one of the simplest strategies, its implementation for driving an SRM has not been extensively investigated before, and its good performance is apparent. In the competition with more advanced controllers, the P-I controller has generally been regarded as the one most likely to succeed in industrial applications. Simplicity, lower cost, zero steady-state error, ease of implementation, robustness, good speed of response, good stability, and other desirable features that made P-I speed controller to succeed in industrial applications [62].

Our control objective is to track a reference speed trajectory. Each phase is provided with current during the torque productive period of rotation and the amplitude of the current is adjusted such that the desired level of torque is obtained. This desired level is dictated by an external feedback loop for controlling the speed. The P-I controller compares the actual speed of the drive and the required speed signal set by the user. The controller output is the torque desired.

We define the motor speed tracking error to be the difference between the reference speed and the plant actual speed. Thus the error is given by:

$$e = \omega_d - \omega \quad (3.22)$$

Where ω_d is a scalar representing the desired motor speed, and ω is the actual motor speed. The primary concern of the controller is to adjust the input signal such that the plant actual speed follows the reference speed. In other words, e is required to be kept as close as possible to the point $e = 0$.

3.4.1 Performance and specifications

Accuracy is measured in terms of the steady state error between the step command input and output variable. The response time of a drive system is defined as the time taken by the system output to reach about 90% of the input speed reference command signal. In other word, it shows how fast a system can respond to changes in the input conditions. Robustness requires that the overall control system be relatively insensitive to external and/or internal disturbances.

The speed regulation (speed tracking capabilities) of a drive system is the ability of the drive to maintain the preset speed under varying load conditions. In many industrial applications it is imperative that the system respond quickly to a load disturbance and maintain a steady constant speed.

For certain processes and certain given inputs, the proportional-integral controller can lead to zero steady state error, good speed of response and stability if the controller parameters are well tuned. However, in some situations, it may be sensitive to changes in the system parameters and/or external disturbances as they are strongly based on the dynamics of the system being controlled. Dynamic system parameters can change due to operating conditions and also due to component aging over the lifetime of the system. The load can

also vary, and sometimes one controller must be able to handle a variety of different loads [62]. The transient performance can be adjusted to satisfy the systems specifications by adjusting the proportional and integral gain constants of the controller, i.e. K_P and K_I .

3.4.2 Speed Controller

The parameters of the proportional-integral controller need to be adjusted to effectively control the process whose dynamics are described by a set of differential equations. As was shown in the beginning of this chapter, the drive control incorporates four hysteresis control loops for the phase currents. By properly designing the P-I controller, it is possible to make the transient response to a step input exhibit relatively small or no overshoot. In the design of the speed controller, the time response of the current loop will be assumed to be so fast that the current reference will be considered to coincide with the actual currents.

The response of a system can be easily analyzed if the system could be approximated by a second order system. Therefore, for simplicity in the analysis, the electrical time constant of the motor is neglected, as the mechanical time constant of that motor is usually much larger than its electrical time constant.

In designing the speed controller we aim to have no more than 5% overshoot and that the rise time should be less than 5 milliseconds. A damping ratio $\zeta = 0.7$ of the model will meet the overshoot requirement and for this damping ratio, a rise time of about 5 milliseconds suggests an undamped natural frequency of about $\omega_n = 400$ rad/sec. Most systems being analyzed for control

system design are much more complicated than the basic second-order system. Approximating the system by a second order model would be used only for guidance.

Since the mechanical time constant of the motor is much higher than the electrical time constant, the governing electromechanical equation of the switched reluctance motor (the dynamic equation of the mechanical subsystem) can be simplified as [63]:

$$J \frac{d\omega}{dt} + B\omega = T_d - T_l \quad (3.23)$$

Since T_d is the output of the controller, for any speed error signal e it is calculated by the speed controller using the following equation:

$$T_d = K_p e + K_i \int e dt \quad (3.24)$$

Using e as it is defined in equation (3.22) and substituting the above expression for T_d in equation (3.23), we get the following closed-loop system:

$$J \frac{d\omega}{dt} + B\omega = K_p(\omega_d - \omega) + K_i \int (\omega_d - \omega) dt - T_l \quad (3.25)$$

where

ω = the actual speed of the motor

ω_d = the desired speed of the motor

J = the moment of inertia

B = the coefficient of friction

K_p = the proportional gain of the speed controller

K_I = the integral gain of the speed controller

T_l = the load torque

T_d = the desired torque

It is assumed that the load torque T_l and the desired speed ω_d are constant and thus their derivatives are zero. After differentiating equation (3.25) with respect to time, we obtain:

$$J \frac{d^2 \omega}{dt^2} + (B + K_p) \frac{d\omega}{dt} + K_I \omega = K_I \omega_d \quad (3.26)$$

A state-space representation of the whole closed-loop drive system using the phase variables is adopted. This can be written as:

$$\begin{bmatrix} \dot{x}_1 \\ \dot{x}_2 \end{bmatrix} = \begin{bmatrix} 0 & 1 \\ -\frac{K_I}{J} & -\frac{B + K_p}{J} \end{bmatrix} \begin{bmatrix} x_1 \\ x_2 \end{bmatrix} + \begin{bmatrix} 0 \\ \frac{K_I}{J} \end{bmatrix} \omega_d$$

$$\omega = \begin{bmatrix} 1 & 0 \end{bmatrix} \begin{bmatrix} x_1 \\ x_2 \end{bmatrix}$$

where

$$x_1 = \omega$$

$$x_2 = \frac{d\omega}{dt}$$

The output variable is the mechanical angular velocity

The transfer function between the input and the output of the closed-loop system is given by:

$$G(s) = c(sI - A)^{-1}b \quad (3.27)$$

where

$$A = \begin{bmatrix} 0 & 1 \\ -\frac{K_I}{J} & -\frac{B + K_P}{J} \end{bmatrix}$$

$$b = \begin{bmatrix} 0 \\ \frac{K_I}{J} \end{bmatrix},$$

$$c = [1 \ 0]$$

I and s are the identity matrix and the complex variable of the Laplace transform, respectively. Therefore, for the whole system (closed-loop system) we get:

$$G(s) = \frac{\frac{K_I}{J}}{s^2 + (\frac{B + K_P}{J})s + \frac{K_I}{J}} \quad (3.28)$$

Using B and J as in Appendix I, then the characteristic equation is given by:

$$s^2 + (625K_P + 2.5)s + 625K_I = 0 \quad (3.29)$$

Thus

$$625K_P + 2.5 = 2\zeta\omega_n \quad (3.30)$$

$$625K_I = \omega_n^2 \quad (3.31)$$

For $\zeta = 0.7$ and $\omega_n = 400$ rad/sec, we get $K_P = 0.892$ and $K_I = 256$. The above parameters would correspondingly be changed, if a different design criterion is selected.

CHAPTER 4

SIMULINK MODEL IMPLEMENTATION AND OFF-LINE AND REAL-TIME SIMULATION

The dynamic equations representing the SRM drive based on which the simulation model is developed are presented in this chapter. The details of the computer model used to simulate the SRM drive system is described in the next section. Also the various steps involved in developing the software for the SRM drive control scheme are discussed and the simulation results are presented. Finally, the design and implementation of the real time model with the real time simulation results are presented in this chapter.

4.1 Dynamic Equations of The SRM Drive

The equations representing the dynamics of the system are formulated, in order to develop a simulation model of the drive system. A set of non-linear first order differential equations govern the operation of the switched reluctance motor, solving these equations the performance of the drive can be obtained. A voltage equation that accounts for the applied voltage, resistive and inductive drops and the rotational Electro Motive Force, represent each phase of the SRM. The various phases of a 4-phase motor are represented by four first order non-linear differential equation, which are decoupled [23].

The voltage equation for the conducting phase is given by,

$$v = Ri + l \frac{di}{dt} + \frac{d\psi(\theta, i)}{dt} \quad (4.1)$$

where, v is the voltage applied across the winding in V, R is the phase resistance in Ω , ' l ' is the phase leakage inductance in H, $\psi = L(\theta, i) * i$, is the flux linkage in wb-turns, where, $L(\theta, i)$ is the self-inductance of the phase in H, i is the phase current in A.

In equation (4.1), the first term in the right-hand side represents the resistive drop. The second term in the right-hand side, which basically represents the leakage inductance drop is usually very small and can be neglected.

The third term is defined as 'e' and is given by,

$$e = \frac{d\psi(\theta, i)}{dt} = \frac{d\psi(\theta, i)}{d\theta} \frac{d\theta}{dt} + \frac{d\psi(\theta, i)}{di} \frac{di}{dt} \quad (4.2)$$

where, θ and i are independent variables.

Hence,

$$e = \frac{d\psi(\theta, i)}{dt} = \frac{d(L(\theta, i)i)}{dt} = \frac{d(L(\theta, i)i)}{d\theta} \frac{d\theta}{dt} + \frac{d(L(\theta, i)i)}{di} \frac{di}{dt} \quad (4.3)$$

$$e = i \frac{dL(\theta, i)}{d\theta} \omega + i \frac{dL(\theta, i)}{di} \frac{di}{dt} + L(\theta, i) \frac{di}{dt} \quad (4.4)$$

In (4.4), the second term can be neglected, since it is negligibly small for low voltage, and high current machines. From equation (2.8), the expression for $L(\theta, i)$ is used in (4.4) to derive a closed form solution for term 'e', which is given by the following equation.

$$e = -\frac{N_r}{2} i \omega [(L_a(i) - L_u) \sin N_r \theta + (L_a(i) + L_u - 2L_m(i)) \sin 2N_r \theta] + \frac{di}{dt} \left[\frac{1}{2} \left(\frac{1}{2} (L_a^*(i) + L_u) + L_m^*(i) \right) + \frac{1}{2} (L_a^*(i) - L_u) \cos N_r \theta + \frac{1}{2} \left[\frac{1}{2} (L_a^*(i) + L_u) - L_m^*(i) \right] \cos 2N_r \theta \right] \quad (4.5)$$

Where,

$$L_a^*(i) = \sum_{n=0}^{n=k} (n+1) a_n i^n \quad (4.6)$$

$$L_m^*(i) = \sum_{n=0}^{n=k} (n+1) b_n i^n \quad (4.7)$$

Similarly, a closed form solution for the electromagnetic torque is derived from the coenergy relations and is given by:

$$T = \int_0^i \frac{\partial \psi}{\partial \theta} di \quad (4.8)$$

$$T = -\frac{N_r i^2}{4} [(L_a^{**}(i) - L_u) \sin N_r \theta + (L_a^{**}(i) + L_u - 2L_m^{**}(i)) \sin 2N_r \theta] \quad (4.9)$$

where,

$$L_a^{**}(i) = \sum_{n=0}^{n=k} \frac{2a_n}{n+2} i^n \quad (4.10)$$

$$L_m^{**}(i) = \sum_{n=0}^{n=k} \frac{2b_n}{n+2} i^n \quad (4.11)$$

The mechanical equations of the drive system are given by,

$$T_d - T_L = J \frac{d\omega}{dt} + B \omega \quad (4.12)$$

$$\omega = \frac{d\theta}{dt} \quad (4.13)$$

where, T_L is the load torque, which can be any function of the angular speed or position, and J is the angular moment of inertia of all the rotating masses, kg m^2 .

The same set of equations with respective currents and phase shifts, represent the other phases. The sum of the instantaneous torques of the individual phases gives the total electromagnetic torque developed by the motor. By solving equations (4.1), (4.12) and (4.13) simultaneously, the performance of the motor can be obtained. This completes the development of the dynamic equations for the SRM.

4.2 Description of The Dynamic Model of The SRM Control Drive

Once the static characteristics of the motor are modeled accurately, the performance of the SRM drive can be predicted through computer simulations. The static characteristics of the motor are represented using the inductance

model of the motor described in chapter 2. In order to simulate the drive performance, Matlab/Simulink package is used in this research. The SRM dynamic equations presented in the previous section are modeled in Simulink and solved to obtain the drive performance.

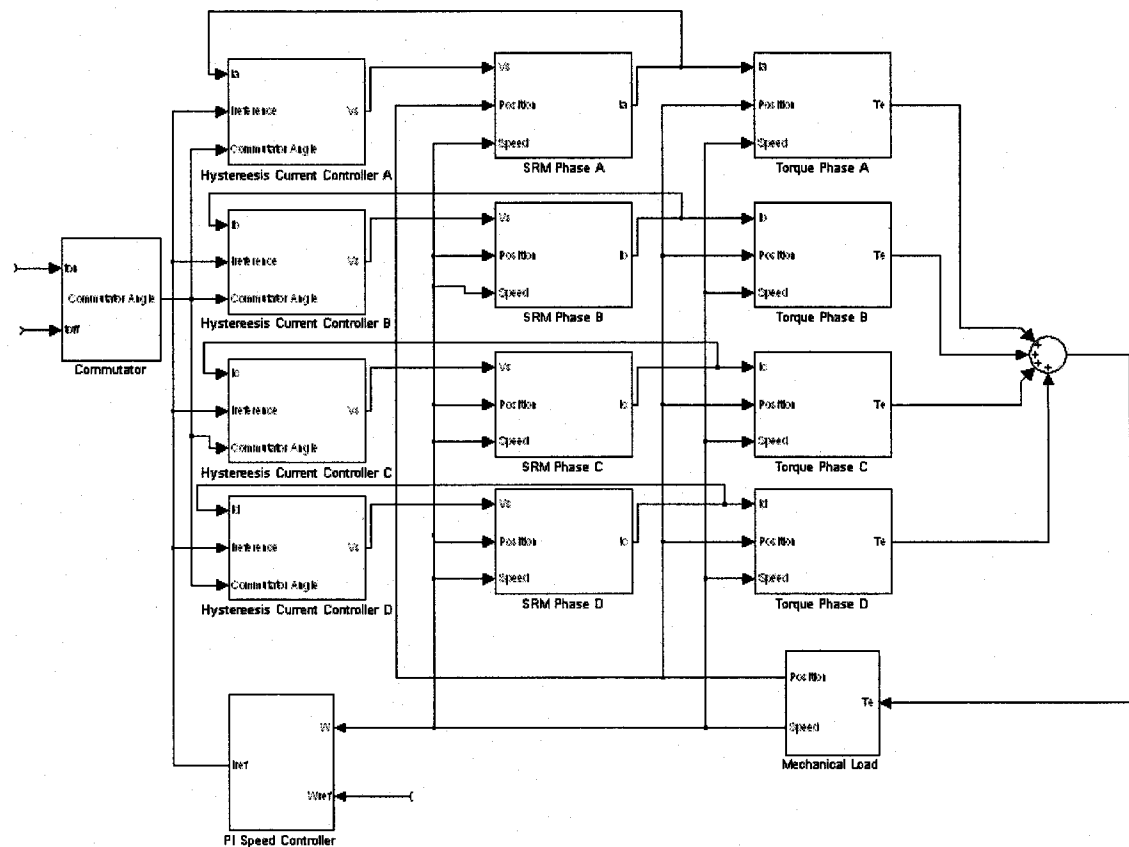


Figure 4.1: Block schematic of the SRM drive control system used for simulation

The above figure shows the block schematic of the drive control system used for simulation. The simulation model comprises of several blocks, and each block is used to carry out a specific task. Each phase of the motor comprises of a hysteresis control block, which simulates the current controller and generates the switching function for the respective phase; a SRM phase block, which

computes the rotational emf and the phase current; a torque block, which computes the torque developed by the respective phase. There is a common mechanical block, which adds up all the individual phase torques to compute the overall electromagnetic torque.

In the mechanical block, any type of load can be modeled and also the other mechanical properties of the drive system like the rotational moment of inertia, friction, etc. can be modeled. Angular acceleration, speed and position are the outputs of the mechanical block, which can be used for feedback purposes.

The Simulink model used in this research basically simulates the speed and current controller for the SRM drive system. Various control quantities like the dc bus voltage, current reference, speed reference, turn-on and turn-off angles and the load conditions can all be defined and simulation can be carried out. Through simulation for any specified operating point, the various phase currents, flux-linkages, torques, rotor speed and position can be obtained. A closed loop speed control operation is performed using a PI controller.

Moreover, one of the simulink model blocks is the fuel cell system, which is used for the power supply for the SRM. Two more blocks were added to connect the fuel cell system to the SRM drive. The two blocks are a Current Converter Block and a boost-up DC/DC converter, they are used to convert the four phases currents for the motor to one load current that is used as a feedback for the Fuel cell, and to boost up the Fuel Cell voltage to the required dc voltage that will be used to drive the SRM, respectively.

For simulation purposes, the SR motor model which is used has the following specifications: 90KW, 25,000 RPM, 8/6, four-phase motor. The simulation results will be divided into two sections, offline simulation and real time simulation. Each will be done before and after adding the speed Controller.

4.3 Hysteresis Controller

The hysteresis controller maintains the current waveform between an upper and a lower limit in the hysteresis band. The actual current is fed back to be compared with the reference current. Whenever the actual current exceeds the upper band, the output voltage changes from V to 0 and the current starts to decay. As soon as the current crosses the lower band limit the voltage changes back again and the actual current starts to increase.

By simulating a hysteresis controller, the actual current is forced to follow the reference current. In hysteresis control, the following control law is applied:

$$\text{If } i_{ka} > i_R + i_h, \text{ then } v_k = 0$$

$$\text{If } i_{ka} < i_R - i_h, \text{ then } v_k = +V_{DC}$$

where

i_{ka} = phase actual current

i_R = reference current

i_h = allowed hysteresis band

V_{DC} = the power converter dc bus voltage

4.4 PI Speed Controller

The speed control system introduced in the previous chapter is simulated using the equations described in this chapter. The feedback control system employed for speed control of the switched reluctance motor drive, consists of a Proportional-Integral controller which compares the actual speed of the drive, and the desired speed signal provided by the user. Upon speed demand, the speed controller computes the value of the control signal which is the output of the speed controller using equation (3.24), which yields the desired torque T_d . This command is used to generate the reference current using the following equation.

$$i_R = \sqrt{\frac{2T_R}{K}} \quad (4.14)$$

where

$$K = \frac{L_a - L_u}{\beta_s}$$

i_R = reference Current

L_a = aligned phase inductance

L_u = unaligned phase inductance

β_s = stator pole arc

The following figure shows the speed control simulated system.

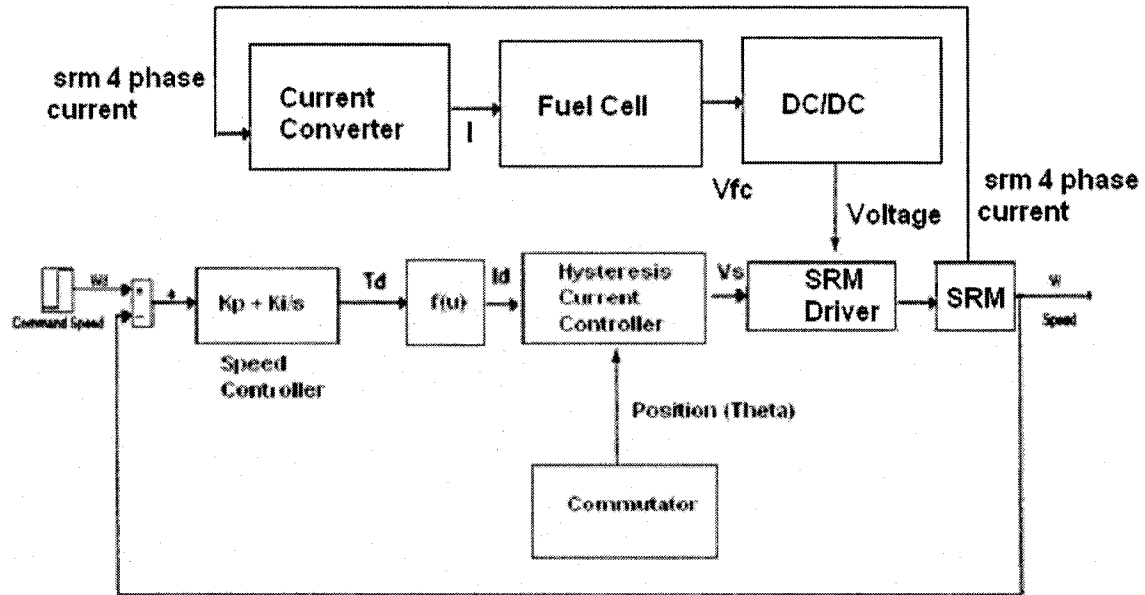


Figure 4.2: Speed controller block diagram

4.5 Offline Simulation Results

The fuel cell voltage is 270V and the current reference is set equal to 600A. Each phase is turned on at its unaligned position and turned off 5° prior to the aligned position. The mechanical load is chosen such that the motor operates in the current controlled mode of operation. Since the motor operates below the base speed, the amplitude of the rotational Electro Motive Force (emf) is small and hence only the current controller regulates the phase current.

While performing simulation, a fixed time step of 40μs was used in order to simulate fixed frequency sampling of 25KHZ. The phase voltages, currents and the switching functions are written into various output files.

In order to simulate the sensorless scheme that was used to design the commutation angle controller, the rotor position estimation algorithm was developed in Matlab. The estimation algorithm reads the active phase voltages,

currents and the switching functions from the files output by simulink. This data was used to solve equations (3.5) and (3.7) in order to obtain the rotor angle.

The simulation was done using a conduction angle of 15° for each phase so that there will be no overlap between the adjacent phase conduction. Each phase is turned on at 7.5° and turned off at 22.5° from the unaligned position respectively. Rotor position is estimated using active phase currents and voltages. The estimated rotor angle is reset to zero whenever any phase starts conducting and each active phase is used for position estimation for 15° . The following figures show the offline simulation results before and after adding the speed controller and it will also show the SRM current results after the Hysteresis controller.

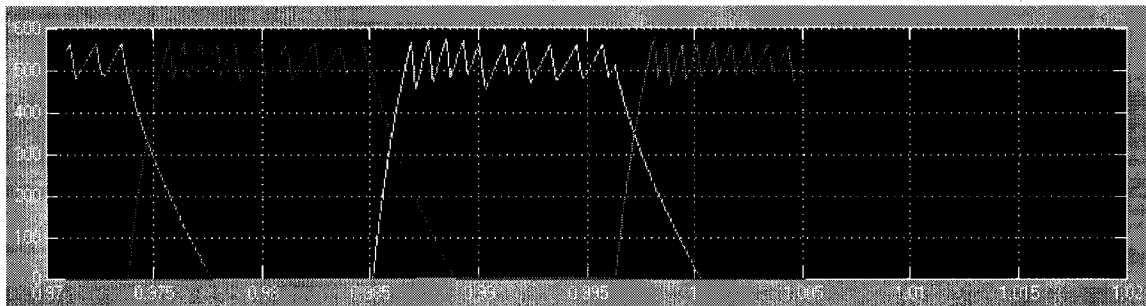


Figure 4.3: four phase SRM current offline simulation

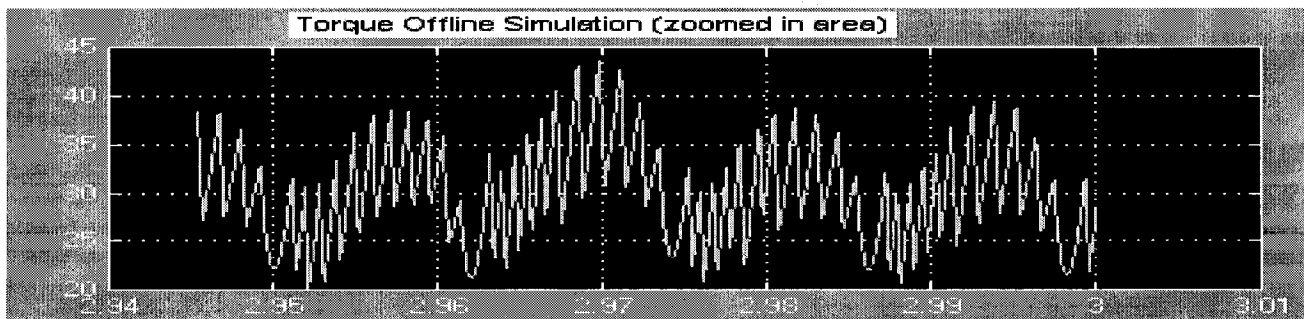


Figure 4.4: Torque Offline Simulation before adding the Speed Controller

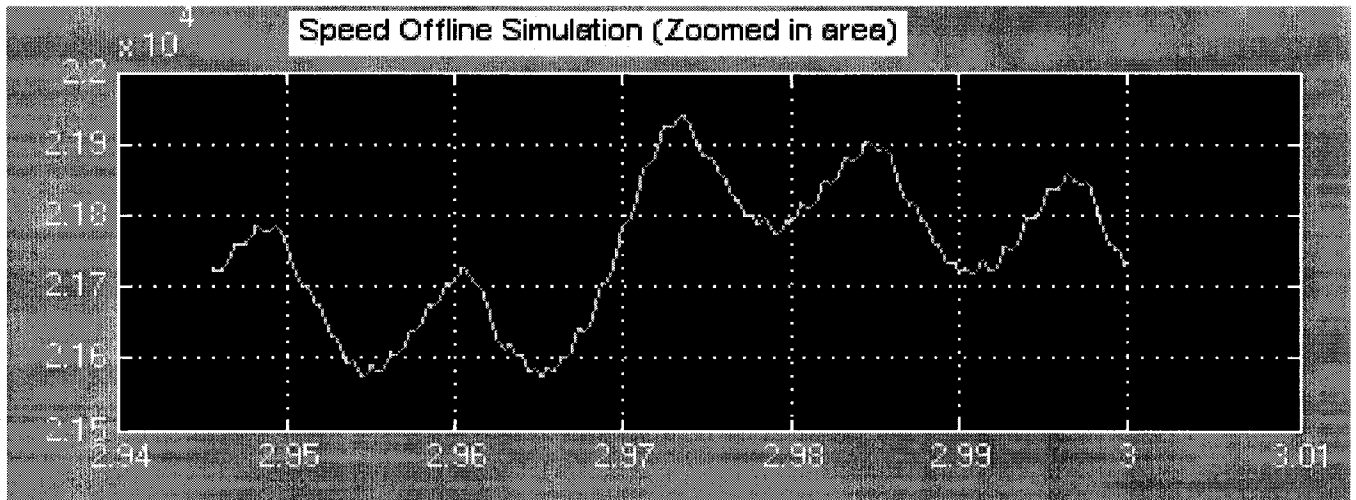


Figure 4.5: Speed Offline Simulation before adding the Speed Controller

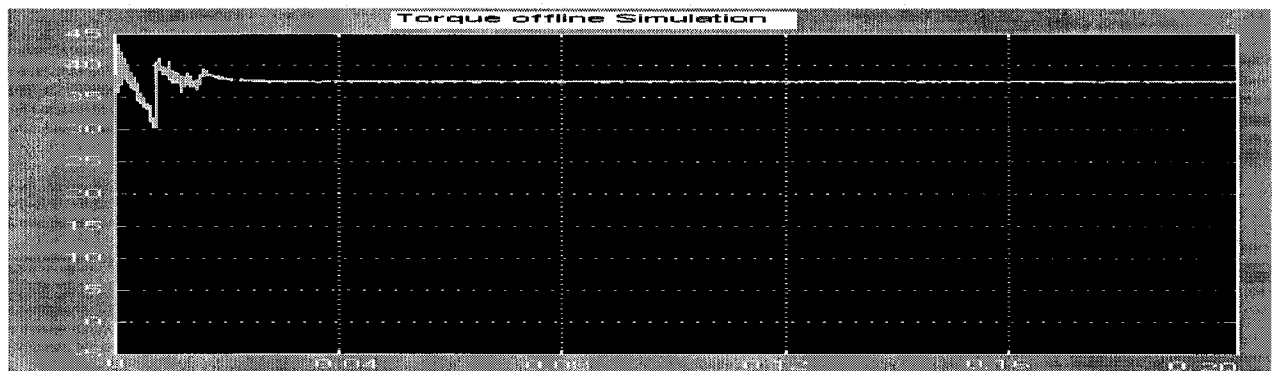


Figure 4.6: Torque Offline Simulation after adding the Speed Controller

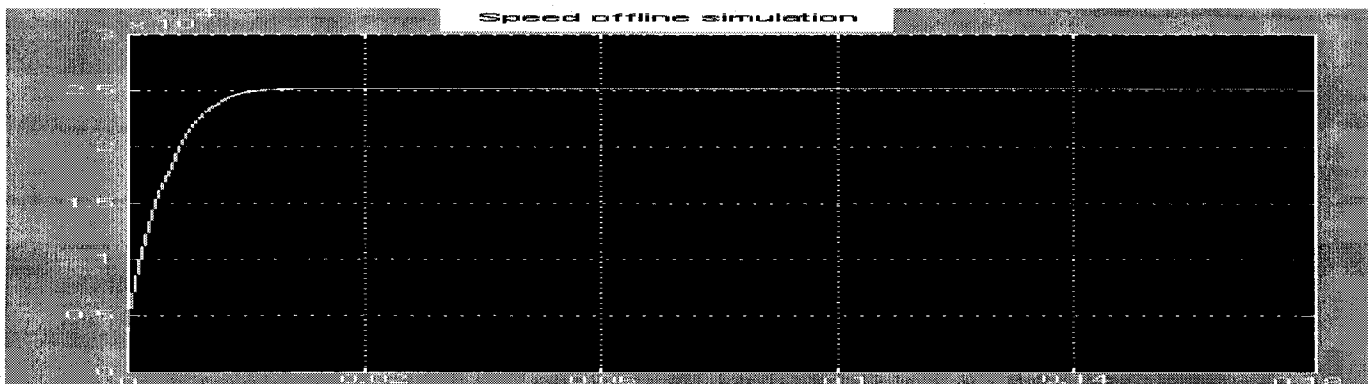


Figure 4.7: Speed Offline Simulation after adding the Speed Controller

From the above figures we can see that before the speed controller the speed and the torque were varying between two values 40 & 20, and 2.195×10^4 & 2.165×10^4 respectively. While, after adding the speed controller they both became stable at one value. The torque became stable at 37.5 and the speed became stable at 2.5×10^4 .

4.6 Real-Time Simulation

In a competitive world, using real-time simulation rather than numerical simulation (offline simulation) provides a significant advantage. Real-Time simulation can minimize risks, improve reliability, and bring a system into operation more quickly, while numerical simulation results may not be reliable, sometimes only qualitative. Opal-RT platform was used to develop the real time simulation for the SRM drive control model developed in this research.

Opal-RT has developed the technology that enables model separation to allow distributed execution, while automatically generating, downloading, and running real-time, high performance, deadlock-free distributed simulation software code. Opal-RT software, which is called RT-LAB software, integrates the most advanced computer, communication, and simulation technologies commercially available in today's industry, to reduce design and implementation time and cost, while increasing scalability and flexibility with no sacrifice in performance.

RT-LAB software runs on a hardware configuration consisting of Command Station, Compilation node, Target nodes, Communication links (real-

time and Ethernet), and the I/O boards. It is configured on Windows platform for the Command Station. Simulations can be run entirely on the Command Station computer, but they are typically run on one or more target nodes. For real-time simulation, the preferred operating system for the target nodes is QNX. When there are multiple QNX nodes, one of them is designated as the compilation node. The Command Station and target node(s) communicate with each other using communication links, and for hardware-in-the-loop simulations target nodes may also communicate with other devices through I/O boards.

4.6.1 Command Station

The command Station is a PC workstation that operates under Windows operating system, and serves as the user interface. The Command Station allows users to:

- Edit and modify models
- See model data
- Run the original model under its simulation software (Simulink)
- Generate code
- Separate code
- Control the simulator's GO/STOP sequences

4.6.2 Target Nodes

The target nodes are real-time processing and communication computers that use commercial processors interconnected by an Ethernet adapter. These computers can also include a real-time communication interface like FireWire or

cLAN (depending on the selected OS), as well as I/O boards for accessing external equipments. The real-time target nodes perform:

- Real-time execution of the model's simulation
- Real-time communication between the nodes and I/Os
- Initialization of the I/O systems
- Acquisition of the model's internal variables and external outputs through I/O modules
- Implementation of user-performed online parameters modifications
- Recording data on local hard drive, if desired
- Supervision of execution of the model's simulation, and communication with other nodes.

4.6.3 Compilation Node

The compilation node is used to:

- Compile C code
- Load the code onto each target node
- Debug the user's source code (S-function, user code block, etc.)

4.6.4 Communication

4.6.4.1 FireWire Real-Time Link

The real-time communication link works using FireWire (IEEE P-1394) or cLAN interfaces. Both ensure:

- Real-time communication between slaves, and between the target nodes and the I/O
- Synchronization between the I/O boards and target nodes.

4.6.4.2 Ethernet Link

An Ethernet link is used to transfer simulation models and run-time data between the Command station and the target nodes

4.6.4.3 I/O boards

Both analog and digital I/O boards are supported by RT-LAB. These allow connection to external equipment for applications such as Hardware-In-Loop.

4.7 Real-Time Simulation for SRM Drive Control

In order to run the SRM drive control Simulink model in RT-LAB software the model must be separated into subsystems and appropriate communication blocks are inserted to connect the model subsystems. Each of the subsystems represents one node in the real-time network. For RT-LAB software there are three types of subsystems that are used to divide any simulink model, which are Console, Master, and Slaves.

The Console subsystem is the station operating under the Windows operating system platform, where we can interact with the system. It contains all the Simulink blocks related to acquiring and viewing data (scope, manual switch,

To workspace-type blocks, etc.). Any Simulink model that will run in RT-LAB platform should have only one Console block.

The Master computation subsystem is responsible for the model's real-time calculation and for the overall synchronization of the network. In a system containing Hardware-in-the-Loop (HIL) this subsystem is also responsible for I/O communication. The Master includes Simulink blocks that represent operations to be performed on signals and/or on Input/Output icons. The Master subsystem for the SRM drive control model contains the Fuel Cell stack model and the Drive Controller block for the SRM. Any Simulink model that will run in RT-LAB platform should have only one Master block.

The Slave computation subsystems are also responsible for performing calculations in the model, and are driven by the Master subsystem, which synchronizes the whole network. Slave computation subsystems contain Simulink blocks that represent operations to be performed on signals. For real-time applications, there can be more than one slave. The number of slaves depends on the simulated model complexity and the number of target nodes availability. For the purpose of this model, only one slave block is used that has the SRM block, SRM drive block, and the Mechanical block. For any Simulink model to run in RT-LAB software it has to run in fixed time step simulation. The following section gives the steps of running the SRM drive control model in RT-LAB software and it shows the real-time simulation results.

4.7.1 Running SRM Drive Control in RT-LAB Software

In order to run the SRM drive control that was developed in this research in RT-LAB software, the following steps were done:

- Offline Simulation model was remodeled to change it from running in variable time step to fixed time step, which was done by changing all the power electronics blocks (Current Converter & SRM chopper) to Simulink IF & ELSE blocks.
- The model was divided into three blocks, Console, Master and Slave and an Opal-RT Lab communication blocks were used to connect the inputs and outputs between these blocks.
- Once the original model has been separated into subsystems, we open the model with RT-LAB software, and we make sure to add the files and values needed to initialize any of the model parameters to RT-LAB Window using the Parameters Configuration Tab.
- Then using the Compilation Tab, the model is automatically coded in C and compiled for execution by the target nodes. Target nodes are commercial PCs, equipped with PC-compatible processors that operate under Windows or QNX environment. In the QNX environment, the real-time sending and reception of data between QNX nodes is performed through FireWire-type communication boards, typically at 200Mb/s or 400Mb/s (depending on the card chosen). In Windows environment, real-time communication takes places using a Giganet Communication device (1200 Mb/s), or shared memory for distributed computing

on a single multiprocessor machine. Less time-critical data can be sent and received through Ethernet communication.

- When the C coding and compilation are complete, RT-LAB automatically distributes its calculations among the target nodes, and provides an interface through the Execution Tab so the model can be executed for the real-time simulation.

- The real-time simulation results were monitored through the Console Block. Communication between the Console and the target nodes is performed through a TCP/IP connection. This allows us to save any signal from the model, for viewing or for offline analysis. It is also possible to use the Console to modify the model's parameters while the simulation is running. The following figures show the real time simulation results for the model before and after adding the speed controller, they also show the SRM current results after the Hysteresis controller.

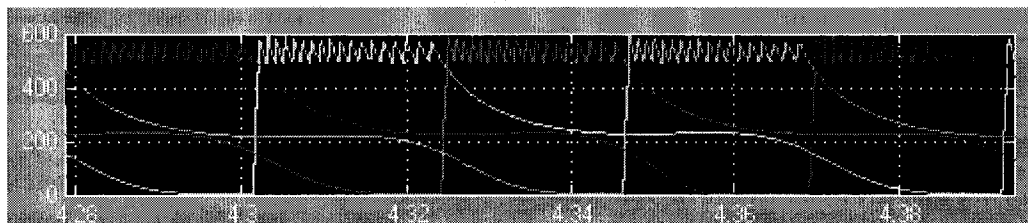


Figure 4.8: Real-time four phase SRM current

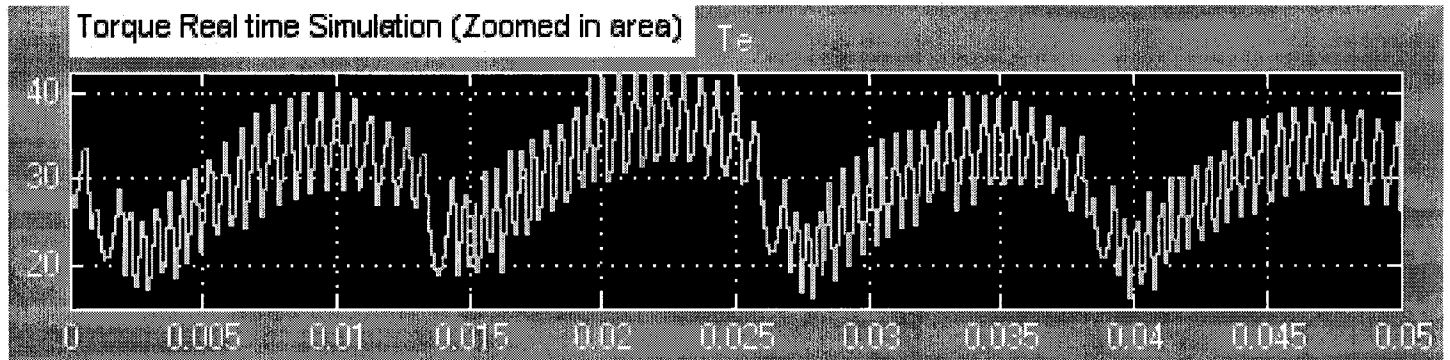


Figure 4.9: Torque Real Time Simulation (Zoomed in area) before adding Speed Controller

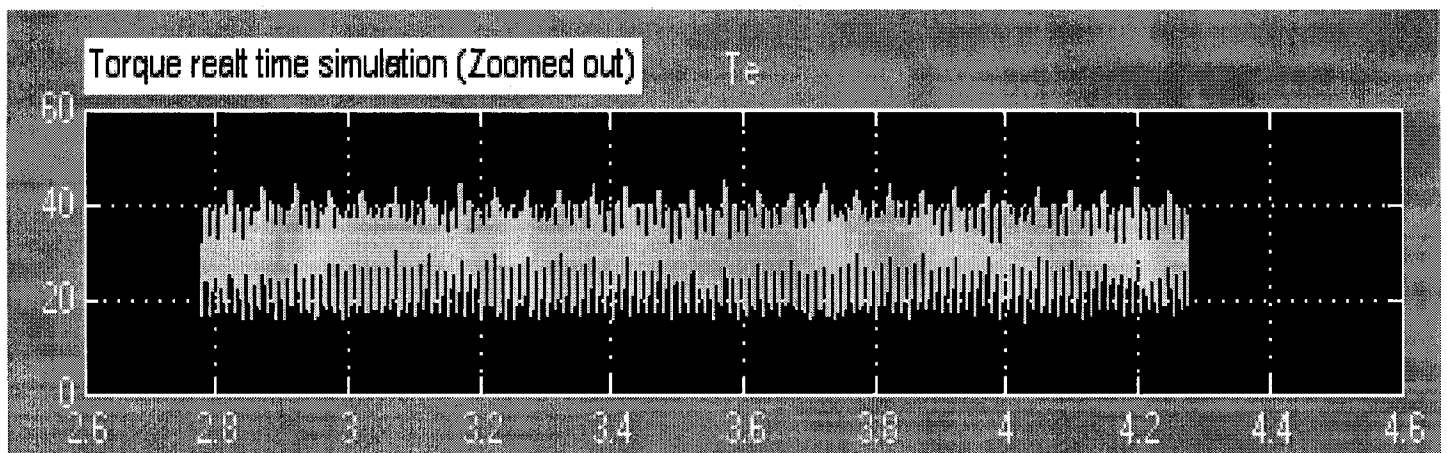


Figure 4.10: Torque Real Time Simulation (Zoomed out area) before adding Speed Controller

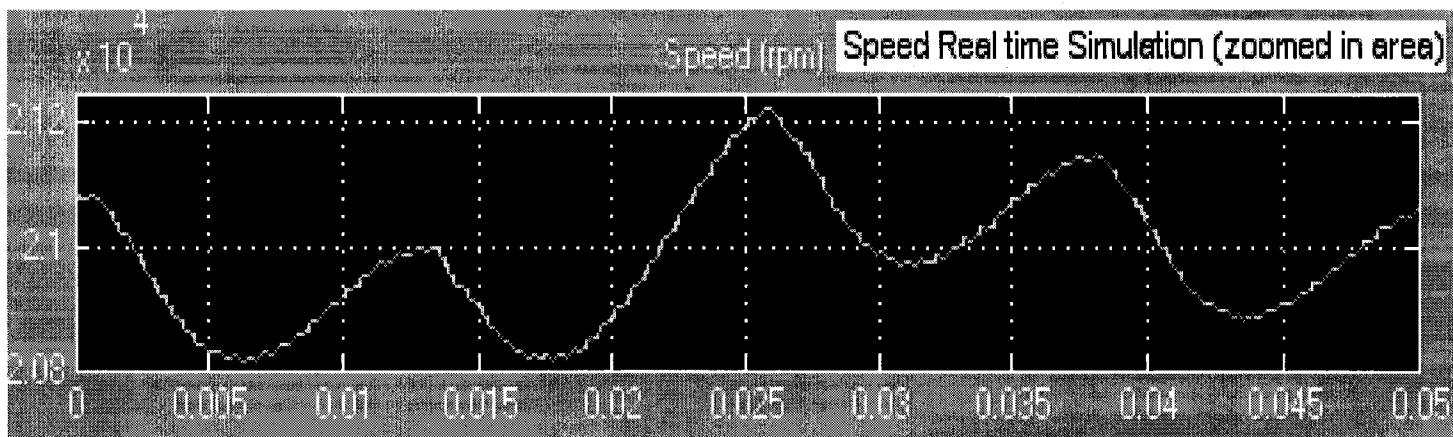


Figure 4.11: Speed Real Time Simulation (Zoomed in area) before adding Speed Controller

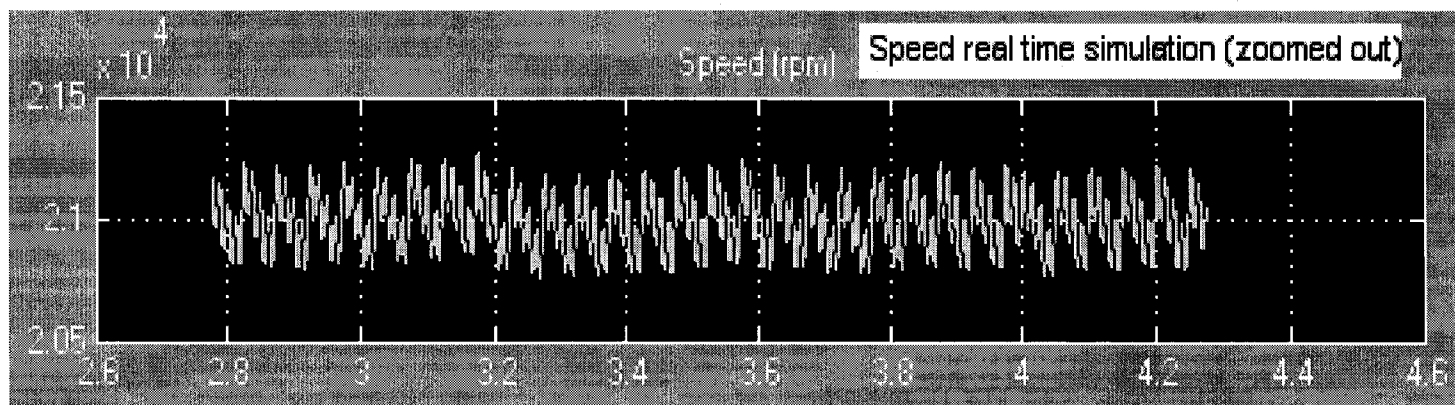


Figure 4.12: Speed Real Time Simulation (Zoomed out area) before adding Speed Controller

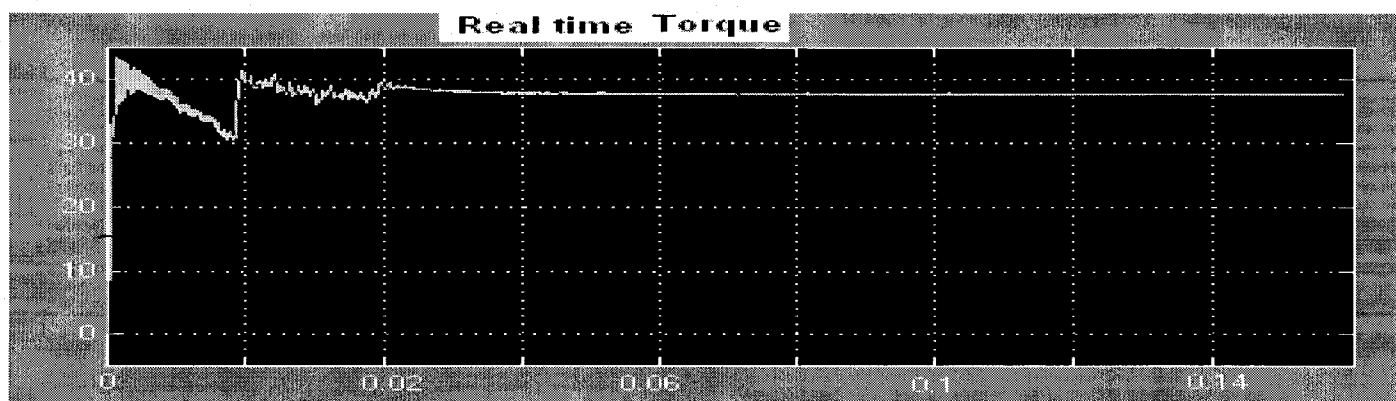


Figure 4.13: Torque Real Time Simulation after adding speed controller

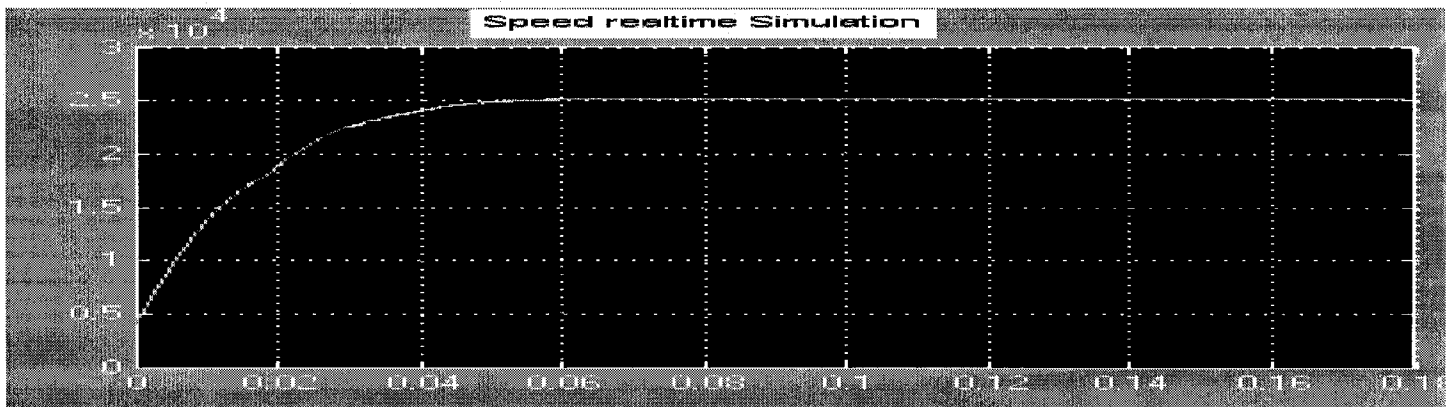


Figure 4.14: Speed Real Time Simulation after adding speed controller

From the above figures we can see that the RT-LAB real-time simulation results are close to the Matlab/Simulink offline simulation results, which concludes that the RT-LAB real-time simulation didn't affect the Simulink drive control model. This proves that the real-time simulation will be a good candidate for the future automotive, industry or research applications using hardware-in-the-loop Simulation.

CHAPTER 5

SUMMARY AND CONCLUSIONS

5.1 INTRODUCTION

Switched reluctance motors have gained increasing popularity in variable-speed drives and have been found competitive with traditional ac and dc drives because of their simple structure, ruggedness, low cost, and the simplicity of the associated power chopper. There is a growing demand for SRM drive systems for such diverse applications as aerospace, robotics, traction and automotive, mining, oil and gas industries, and products such as pumps, fans, and appliances. Moreover, the switched reluctance motor can be designed for low speed and high torque capability. These characteristics make the switched reluctance motor attractive for direct-drive applications. However, its nonlinear electromechanical characteristics and its periodic variation of inductance in each phase result in torque ripple and hence speed ripple. The design of controller for the SRM is quite a challenging problem. P-I controllers are robust and they give good performance at low cost, which made them widely used for motor control. In this concluding chapter, the research work is summarized, advantages and disadvantages of P-I controller are explained, and some suggestions for further research are presented.

5.2 Summary of The Thesis

An introduction and a literature review of the switched reluctance motor were presented in chapter 1. Most of the SRM design models and their drive controllers presented in literature are always depending on using the Finite-Element method in designing the SRM which in turn causes the drive controller model to be complicated in design and hard to simulate in real time. The work presented in this Thesis solves that problem by developing a drive controller for SRM using the inductance model for the motor, which was easily able to simulate in real time platform. In addition to that, this Thesis also presents a Fuel Cell Stack Simulink model that was able to simulate in real time platform, which will be helpful in using it in hardware in the loop for other projects dealing with fuel cell. This will solve the problem of having to use an actual Fuel Cell stack, which is always a concern from the design complexity and cost point of view. The mathematical model of the switched reluctance motor, which gives a better appreciation of the operating characteristics and the control purposes for the motor, was presented in chapter 2.

A speed controller system based on a proportional-integral control strategy was designed in chapter 3. Our control objective is to track a reference speed trajectory. A P-I control law is chosen only because of its very good and desirable features and is not intended to infer that this is the best control law. A feedback control system was employed for speed control of the switched reluctance motor drive to provide the desirable performance. This consists of a P-I controller which compares the actual speed of the drive and the required

speed signal provided by the user. The transient performance can be adjusted to satisfy the system specifications by adjusting the controller constants K_p and K_i .

Performance is based on the ability of the control system to provide each phase with pulses of current during the torque productive periods by selecting predetermined switching angles. The performance and results for the offline and real time simulation were presented in chapter 4. In order to minimize the torque ripple a Hysteresis Current Controller and a commutation system were designed. Where the hysteresis current controller used the reference current value from the P-I Controller to limit the actual current for the SRM to this desired value, while the function of the commutation system is to designate the appropriate phases for torque development and commutation. In this control scheme employed in this study, a single phase is energized at a time, the "on" and "off" angles are fixed at θ_{on} and θ_{off} . The actual phase to be energized is determined by the rotor position.

5.3 Advantages and Disadvantages of P-I Controller

Proportional-Integral controllers have been widely used in industry. In competition with more advanced controller, P-I controllers have generally been regarded as more successful in industrial applications. The main reasons for this have been simplicity, lower cost, zero steady-state error, ease of implementation, robustness, accuracy, good speed of response, and ability to achieve stability.

The integral component of this controller will ensure that the steady-state error is zero for a step change, which is a very useful feature for many

applications. The transient response may not be acceptable, although a P-I controller makes the steady-state error zero. For example, it could increase the settling time. This might not be tolerated in some high-performance applications such as robotics. Nevertheless, a P-I controller can be designed to respond very quickly, but in this case an undesirable speed overshoot may occur. Hence, one has to choose a design suitable to a particular application.

Since P-I controllers are essentially low-pass filters, they can filter out high-frequency noise. P-I controllers are examples of good classical control design techniques. One drawback is that they are strongly based on the dynamics of the system being controlled and in some situations they may be sensitive to changes in the plant parameters and/or external disturbances.

At the present time, many applications use P-I control strategies for speed control, despite some of its disadvantages. However, more advanced control laws could be employed where superior dynamic performance is desired under all motor operating conditions, due to the high nonlinearity of the switched reluctance motor.

5.4 Suggestions For Future Work

The potential for future research work in this area is vast. In this thesis, a simplified SRM dynamic model, which neglects magnetic saturation, was presented and a drive control for the motor was developed and simulated in real time using Fuel Cell as a power source for the motor. For future work, a physical SRM motor can be used in hardware-in-the-loop to be tested with the Fuel cell

model and the Controller model using Opal-RT lab platform. This can improve the accuracy, particularly for high performance applications with low cost.

Some high-performance industrial applications such as robotics and machine tools require variable speed drive systems, which need to be relatively insensitive to parameter variations and/or external disturbances. They also require drive systems that are highly accurate, robust, and fast. To provide such a high degree of performance, more advanced and complex control strategies may be needed to make the system highly robust and accurate.

In this study, the research involved modeling, system design, and simulation. The next step would be to experimentally test these theoretical results. This experimental approach could also be an area for future research.

REFERENCES

- [1] P.J. Lawrenson, J.M. Stephenson, P.T. Blenkinsop, J. Corda, N.N. Fulton, "variable-Speed Switched Reluctance Motors." Proc.IEE, Vol.127, Pt.B, No.4, July, 1980, pp.253-265
- [2] T.J.E. Miller, Switched Reluctance Motor and Their Control, Magna Physics Publishing and Oxford Science Publications, London, 1993.
- [3] "Four quadrant control of a SRM", Dr. Iqbal Husin, Department of Electrical Engineering, University of Akron, SAE August 2-3, 2003
- [4] B.K. Bose, T.J.E. Miller, P.M. Szczensny, W.H. Bicknell, "Microcomputer Control of Switched Reluctance Motor," IEEE Transactions on Industry Applications, Vol. IA-2, July/August, 1986, pp.708-715.
- [5] "Fuzzy Logic Control of a SRM", P. Branco, IEEE 1997
- [6] "Torque Ripple Minimization in a switched reluctance drive by neuro-fuzzy compensation" Luis G. B. Rolim, IEEE September 2000
- [7] Performance simulation of SRM drive system operating with fixed angle control scheme" Virendra k. sharma, A. Chandra, and kamal El Haddad, Département de génie électrique, Montréal (Québec), Canada, Electrimacs 2002, August 18-21
- [8] K. Rajashekara, Sensorless Control in Motor Drives, IEEE Press, Princeton, NJ, 1997.
- [9] D. E. Cameron, J. H. Lang and S.D. Umans, "The Origin and Reduction of Acoustic Noise in Doubly Salient Variable Reluctance Motor," IEEE Transactions on Industry Applications, Vol. IA-28, No. 6, November/December, 1992, pp.1250-1255.
- [10] B. Fahimi, Control of Vibration in Switched Reluctance Motor Drives, Ph.D. Dissertation, Texas A&M University, May, 1999.
- [11] B. Fahimi, G. Suresh, M. Ehsani, "Design Considerations of Switched Reluctance Motors: Vibration and Control Issues," IEEE Industry Application Society Annual Meeting, Phoenix, October, 1999.
- [12] J. Moreira, "Torue Ripple Minimization in Switched Reluctance Motors via Bi-cubic Spline Interpolation," IEEE PESC Conference Records, 1992, pp. 851-856.

- [13] R. Wallace, D. G. Taylor, "Three-phase Switched reluctance Motor Design to Reduce Torque Ripple," Proc. Of International Conference on Electrical Machines, Cambridge, MA, August 1990, pp. 783-787
- [14] A. V. Radun, "Design Considerations for the Switched Reluctance Motor", IEEE Transactions On Industry Applications, Vol. 31, No. 5, September/October 1995.
- [15] W.A. Harris, "Switched Reluctance Motor Position by Resonant Injection," US Patent, 5, 196,775, March 1993.
- [16] J. T. Pukrushpan, Huei Peng, Anna G. Stefanopoulou, "Simulation And Analysis of Transient Fuel Cell System Performance Based on A Dynamic Reactant Flow Model", Proceedings of IMECE2002, ASME International Mechanical Engineering Congress & Exposition, November 17-22, 2002, New Orleans, Louisiana
- [17] M.H. Fronk, D.L. Wetter, D.A. Masten and A. Bosco. PEM fuel cell system solutions for transportation. SAE Paper 2000-01-0373
- [18] K. Jost. "Fuel Cell Concepts and technology", Automotive Engineering International, March 2000.
- [19] A.J. Appleby and F.R. Foulkes, "Fuel Cell Handbook", Van Nostrand Reinhold, New York, 1989.
- [20] W.R. Grove "A Small Voltaic Battery of great energy", Philosophical Magazine, 15:287-293, 1839.
- [21] James Larimine and Andrew Dicks, "Fuel Cell Systems Explained", John Wiley & Sons Inc, West Sussex, England, 2000.
- [22] Sharon Thomas and Marcia Zalbowitz, "Fuel Cells Green Power", Technical report, Los Alamos National Laboratory.
- [23] S. Gopalakrishnan, M. Ehsani, "Inductance Model Based Sensorless Switched Reluctance Motor Drives for High Performance Applications", May 2000.
- [24] M. Ehsani, I. Husain, S. Mahajan, K.R. Ramani, "New Modulation Encoding Techniques for Indirect Rotor Position Sensing in Switched Reluctance Motors", IEEE Transactions on Industry Applications, Vol.30, No.1, January/February, 1994, pp.85-91
- [25] M. Ehsani, I. Husain, A. B. Kulkarni, " Elimination of Discrete Position Sensor and Current Sensor in Switched Reluctance Motor Drives", IEEE

Transactions on Industry Applications, Vol.28, No.1, January/February, 1992, pp. 128-135.

- [26] R.M. Davis, W.F. Ray, R.J. Blacke, "Inverter Drive for Switched Reluctance Motor: Circuits and Component Ratings," Proc.IEE, Vol.128, Pt.B, March, 1981, pp.129-136.
- [27] S. Vukosavic, V.R. Stefanovic, "SRM Inverter Topologies: A Comparative Evaluation", IEEE Transactions on Industry Applications, Vol.27, No.6, November/December, 1994, pp.1034-1047.
- [28] R. Krishnan, "Switched Reluctance Motor Drives", Tutorial Notes, IEEE Industry Applications Society Annual Meeting, San Diego, October, 1996.
- [29] W.D. Harris, J.H. Lang, "A Simple Motion Estimator for Variable Reluctance Motors", IEEE Transactions on Industry Applications, Vol.IA-26, No.2, March/April, 1990, pp.237-243
- [30] Maxwell Technical User's Manual, Ansoft Corporation, Pittsburgh, 1995.
- [31] P. Badrinarayanan, S. Ramaswamy, A. Eggert, and R.M. Moore, "Fuel Cell stack water and thermal management", Impact of variable system power operation. SAE Paper 2001-01-0537.
- [32] S. Ahmed and M. Krumpelt, "Hydrogen from hydrocarbon fuels for fuel cells", International Journal of Hydrogen Energy, 26:291-301,2001.
- [33] J.C. Amphlett, R.M. Baumert, R.F. Mann, B.A. Peppley, and P.R. Roberge, "Performance modeling of the Ballard Mark IV solid Polymer electrolyte fuel cell", Journal of Electrochemical society, 141(1):9-15, 1995.
- [34] S. Birch, "Ford focus on the fuel cell", Automotive Engineering International, pages 25-28, June 2001.
- [35] K. Ohnishi, N. Matsui, Y. Hori, "Estimation, Identification and Sensorless Control in Motion Control Systems", Proceedings of the IEEE, Vol. 82, No.4, August, 1994, pp.1253-1265.
- [36] J.T. Bass, M. Ehsani, T.J.E. Miller, "Robust Torque Control of Switched Reluctance Motors Without a Shaft Position Sensor," IEEE Transactions on Industrial Electronics, Vol.IE-3, May/June, 1987, pp.212-216.
- [37] S. Vukosavic, L. Peric, E. Levi, V. Vukovic, "Sensorless Operation of the SR Motor with Constant Dwell," IEEE PESC Conference Records, 1990, pp. 451-454

- [38] P.P. Acarnley, R.J. Hill, C.W. Hooper, "Detection of Rotor Position in Stepping and Switched Motors by Monitoring Current Waveforms," IEEE Transactions on Industrial Electronics, Vol. IE-32, No.3, May/June, 1985, pp.215-222.
- [39] S.R. Mac Minn, W. J. Rzesos, P.M. Szczensny, T.M. Jahns, "Application of Sensor Integration Techniques to Switched Reluctance Motor Drives," IEEE Transactions on Industry Applications, Vol.28, No.6, November/December, 1992, pp.1339-1344.
- [40] W.D. Harris, J.H. Lang, "A Simple Motion Estimator for Variable Reluctance Motors," IEEE Transactions on Industry Applications, Vol.IA-26 No.2, March/April, 1990, pp.237-243.
- [41] M. Ehsani, I. Husain, S. Mahajan, K.R. Ramani, "New Modulation Encoding Techniques for Indirect Rotor Position Sensing in Switched Reluctance Motors," IEEE Transactions on Industry Applications, Vol.30, No.1, January/February, 1994, pp.85-91.
- [42] I. Husain, Sensor Elimination and Converter Topology Simplification in Switched Reluctance Motor Drives for Commercial Applications, Ph.D. Dissertation, Texas A&M University, May 1993.
- [43] P. Laurent, M. Gabsi, B. Multon, "Sensorless Rotor Position Detection Using Resonant Method for Switched Reluctance Motors," IEEE Industry Application Society Annual Meeting, 1990, pp.687-694.
- [44] M. Ehsani, I. Husain, A.B. Kulkarni, "Elimination of Discrete Position Sensor and Current Sensor in Switched Reluctance Motor Drives," IEEE Transactions on Industry Applications, Vol.28, No.1, January/February, 1992, pp.128-135.
- [45] M. Ehsani, "Position Sensor Elimination Technique for the Switched Reluctance Motor Drive," US Patent 5,072,166, March 1992.
- [46] W. A. Harris, "Switched Reluctance Motor Position by Resonant Injection," US Patent, 5,196,775, March 1993
- [47] K.R. Ramani, M. Ehsani, "New Commutation Methods in Switched Reluctance Motors Based on Active Phase Vectors," IEEE PESC Conference Records, 1994, pp.493-499.
- [48] K.R. Ramani, "Inductance and Active Phase Vector Based Torque Control for Switched Reluctance Motor Drives", Ph.D. Dissertation, Texas A&M University, December 1994.

- [49] J.P. Lyons, S.R. Mac Minn, M.A. Preston, "Flux-Current Methods for SRM Rotor Position Estimation," IEEE Industry Application Society Annual Meeting 1991, pp.482-487.
- [50] M.T. DiRenzo, W. Khan, "Self-Trained Commutation Algorithm for an SR Motor Drive System Without Position Sensing," IEEE Industry Applications Society Annual Meeting New Orleans, October, 1997, pp.482-487.
- [51] B.G. Hedlund, "Method and a Device for Sensorless Control of a Reluctance Motor," US Patent No. 5,173,650, August 1992.
- [52] A. Lumsdaine, J.H. Lang, "State Observers for Variable-Reluctance Motors," IEEE Transactions on Industrial Electronics, Vol.37, No.2, April, 1988, pp.133-142.
- [53] C. Elmas, H.Z. De La Para, "Position Sensorless Operation of a Switched Reluctance Drive Based on Observer," European Power Electronics Conference, Vol.6, 1993, pp.82-87.
- [54] A. Brosse, G. Henneberger, "Sensorless Control of a Switched Reluctance Motor Using a Kalman Filter," European Power Electronics Conference, Vol.4, 1997, pp.4.561-4.566
- [55] I. Husain, S. Sodhi, M. Ehsani, "A Sliding Mode Observer Based Controller for Switched Reluctance Motor Drives," IEEE Industry Application Society Annual Meeting, 1994, pp.635-643.
- [56] I. Husain, M. Ehsani, "Rotor Position Sensing in Switched Reluctance Motor Drives by Measuring Mutually Induced Voltages," IEEE Transactions on Industry Applications, Vol.30, No.3, May/June, 1994, pp.665-672.
- [57] A. Kawamura, "Survey of Position Sensorless Switched Reluctance Motor Control," IEEE Industry Application Society Annual Meeting, 1994, pp.1595-1598.
- [58] W.F. Ray, I.H. Al-Bahadly, "Sensorless Methods for Determining the Rotor position of Switched Reluctance Motors," European Power Electronics Conference, Vol.4, 1993, pp.7-13
- [59] M. Ehsani, A.V. Rajarathnam, G. Suresh, B. Fahimi, "Sensorless Control of Switched Reluctance Motors- A Technology Ready for Applications," International Conference on Electrical Machines, Istanbul, August, 1998.
- [60] Ooi, H.S., Green, T.c., "Sensorless Switched Reluctance Motor Drive with Torque Ripple Minimization," Proceedings of Power Electronics Specialists Conference, 2000, vol. 3, pp: 1538-1543

- [61] F.R. Salmasi, B. Fahimi, H. Gao, M. Ehsani, "Robust Sensorless rotor Position detection in SRM drives", Power Electronics Specialist Conference, PESC 2001, Vol. 2, pp. 1226-1231, 2001.
- [62] "Modeling and Implementation of Controller for Switched Reluctance Motor with AC Small Signal Model", Xiaoyan Wang, Faculty of the Virginia Polytechnic Institute and State University. October 2001.
- [63] G. John, "Robust Speed Control of the Switched Reluctance motor", Ph.D. Thesis, Department of Electrical & Computer Engineering, Queen's University, 1994.
- [64] M. Ilic' – Spong, R. Marino, S. M. Presada, and D. G. Taylor, "Feedback linearizing control of switched reluctance motors", IEEE Transactions on Automatic Control, Vol. AC-32, No. 5, pp.371-379, May 1987
- [65] M. Ilic'-Spong, T.J.E. Miller, S.R. Mac Minn, and J.S. Thorp, "Instantaneous torque control of electric motor drives", IEEE Transactions on Power Electronics, Vol. PE-2, No.1, pp.55-61, January 1987
- [66] S. Bobognani, and M. Zigliotto, "Fuzzy logic control of a SRM drive", IEEE Transactions on Industry Applications, Vol. 32, No.5, pp.1063-1068, September/October 1996.
- [67] R. R. Kohan, and S. A. Bortoff, " Adaptive control of variable reluctance motors using spline functions", Proc. Of the 33rd Conf. on Decision and Control, pp. 1694-1699, December 1994.
- [68] S. K. Panda, and P. K. Dash, "Application of nonlinear control to SRMs: a feedback linearization approach", IEE Proceedings, Electr. Power Appl., Vol. 143, No.5, pp.371-379, September 1996
- [69] L.A. Belfore, and A.A.Arkadan, "Modeling faulted SRMs using evolutionary neural networks", IEEE Transactions on Industrial Electronics, Vol.44, No.2, pp.226-233, April 1997.

APPENDIX A

SRM Inductance Model

The following will show the equations and values that were developed in Dr. Ehsani's work to design the SRM Inductance model. The phase inductance equation is given by,

$$L(i, \theta) = L_0(i) + L_1(i)\cos(N_r\theta) + L_2(i)\cos(2N_r\theta) \quad (A.1)$$

where,

$$L_0(i) = \frac{1}{2} \left[\frac{1}{2} (L_a(i) + L_u) + L_m(i) \right] \quad (A.2)$$

$$L_1(i) = \frac{1}{2} (L_a(i) - L_u) \quad (A.3)$$

$$L_2(i) = \frac{1}{2} \left[\frac{1}{2} (L_a(i) + L_u) - L_m(i) \right] \quad (A.4)$$

where,

$$L_a(i) = L(\theta = 0^\circ) = \sum_{n=0}^{n=k} a_n i^n \quad (A.5)$$

$$L_m(i) = L(\theta = \frac{\pi}{2N_r}) = \sum_{n=0}^{n=k} b_n i^n \quad (A.7)$$

$$L_u = L(\theta = \frac{\pi}{N_r}) \quad (A.6)$$

The polynomial coefficients obtained are shown below:

$$a_0 = 0.00095885$$

$$a_1 = -0.4369057e-5$$

$$a_2 = 0.6471747e-7$$

$$a_3 = -0.2731239e-7$$

$$a_4 = 0.3648079e-9$$

$$a_5 = -0.1589331e-11$$

$$b_0 = 0.000442262$$

$$b_1 = -0.1368487e-5$$

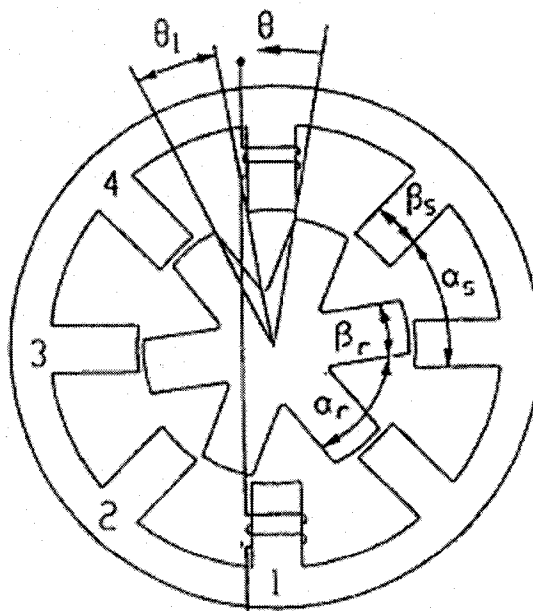
$$b_2 = 0.1632494e-6$$

$$b_3 = -0.5953759e-8$$

$$b_4 = 0.7181161e-10$$

$$b_5 = -0.2897464391e-12$$

The following figure shows the structure of a four-phase SRM:



SRM Geometry table used by Dr. Ehsani's work

Parameter	Value
Stator Diameter	140 mm
Rotor Diameter	69.6 mm
Stack Length	80 mm
Stator arc	22.5° (mech)
Rotor arc	22.5° (mech)
Air gap length	0.3 mm
Shaft diameter	18.8 mm
Stator back iron	9 mm
Rotor back iron	12 mm
Number of windings per phase	20

List of Symbols

B	Coefficient of friction
e	Speed error
i	Current
i_d, i_r	Desired Current and Reference Current
$\Delta I, I_h$	Hysteresis band
I_{dc}	dc link current

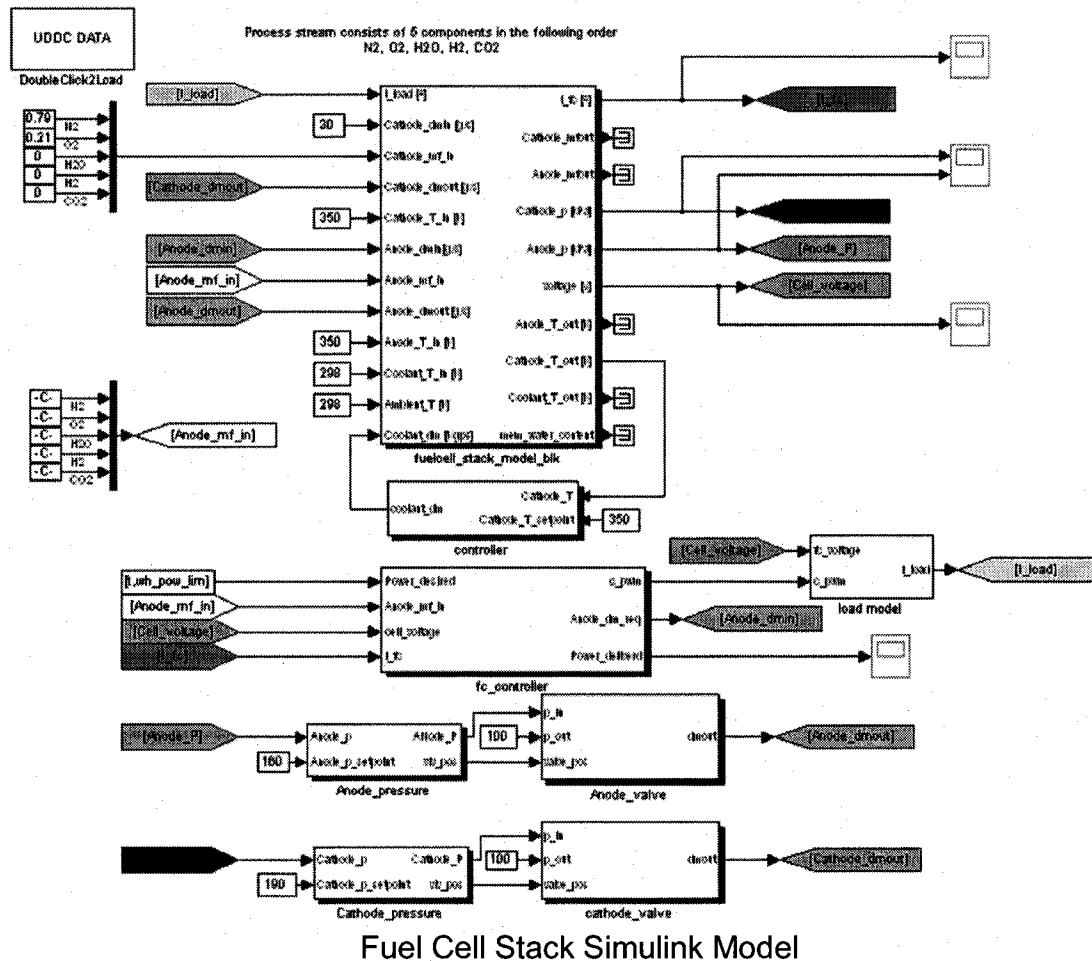
J	Moment of inertia
k	Suffix denoting phases
K	Slope of the inductance profile
K_I	Integral gain of the speed controller
K_P	Proportional gain of the speed controller
$L, L(\theta)$	Phase inductance
L_a	aligned phase inductance
L_u	unaligned phase inductance
N_r	number of rotor poles
N_s	number of stator poles
q	number of phases
R, r	phase resistance
s	complex variable of the Laplace transform
t	time
T	electromagnetic torque
T_d, T_r	Desired torque and Reference torque
T_L	Load torque
v	voltage
V_{dc}	dc link voltage
α_r	rotor pole pitch
β_r	rotor pole arc
β_x	stator pole arc
ζ	damping ratio

θ	rotor position
$\theta_{on}, \theta_{off}$	“on”, “off” angle
ψ	flux linkage
ω	actual speed of the motor
ω_r	reference speed of the motor
ω_n	undamped natural frequency
P-I	Proportional-integral
SRM	switched reluctance motor

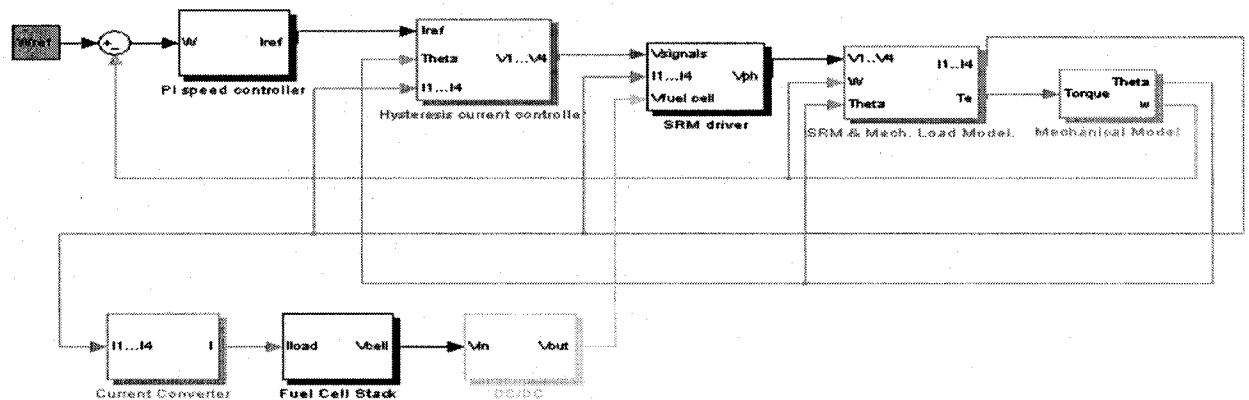
Values used for simulation

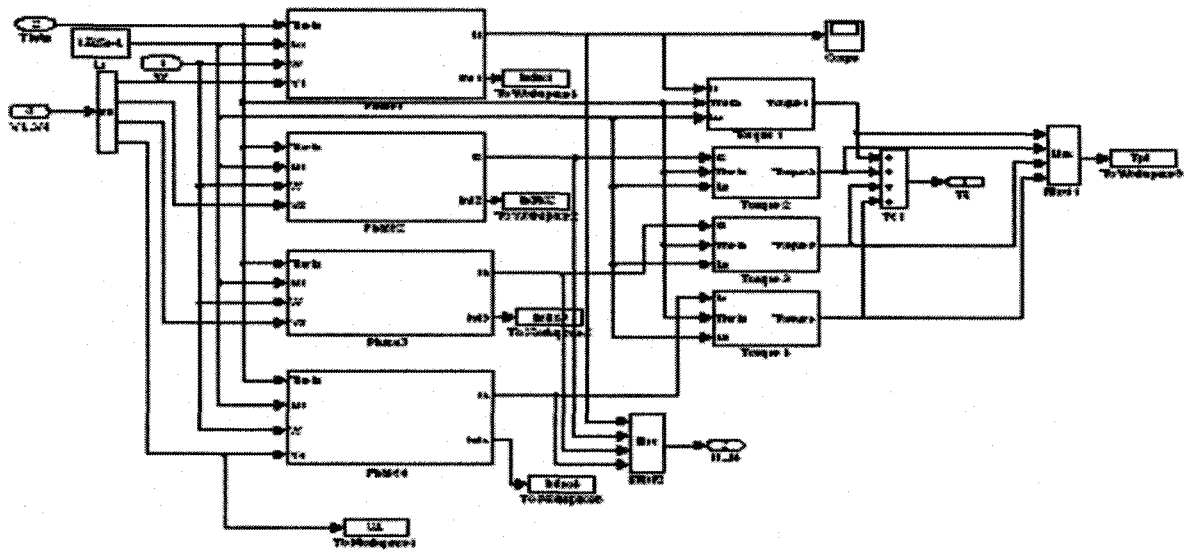
q	4
N_s	8
N_r	6
L_u	10mH
L_a	110mH
β_s	0.35 rad
r	0.95Ω
J	0.0016 kg.m^2
B	0.004 Nm/rad/sec

APPENDIX B

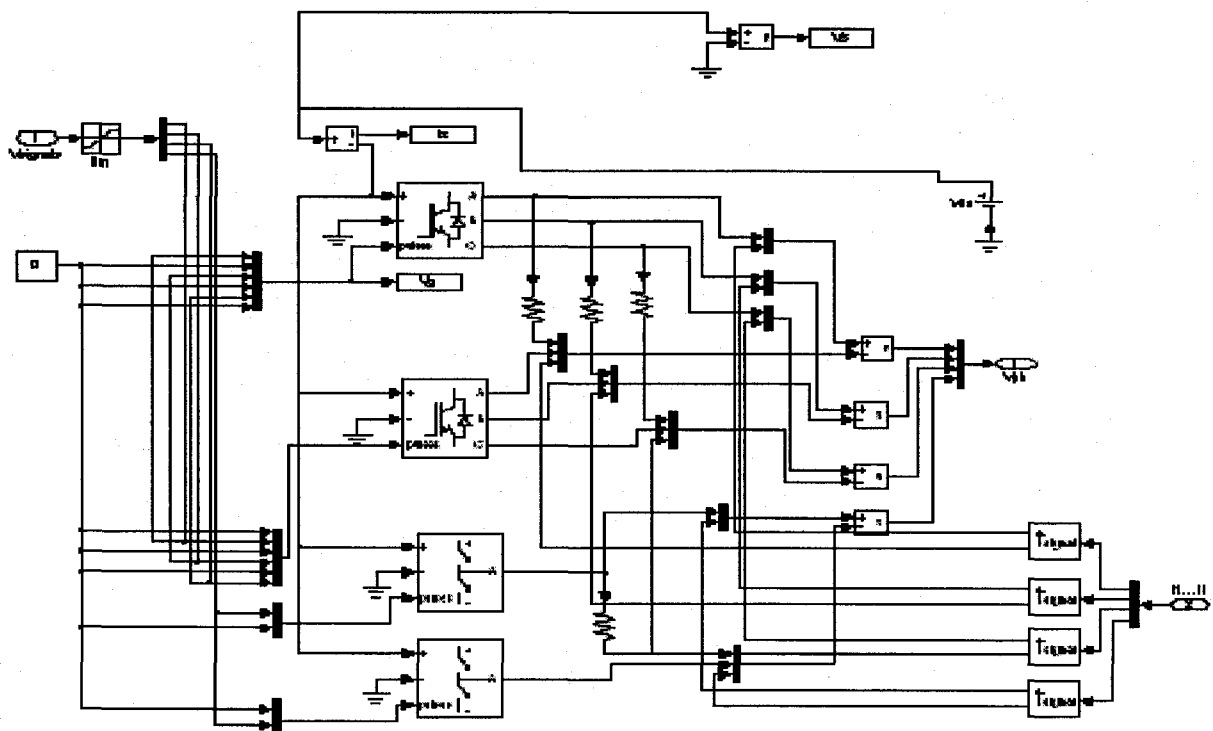


SRM MODEL

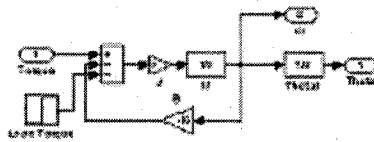




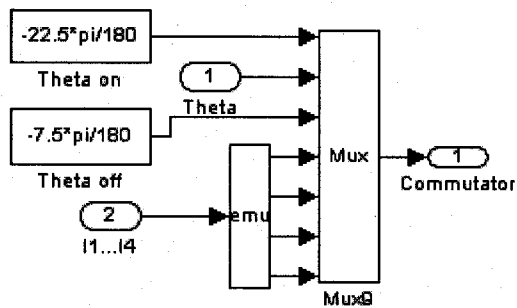
SRM inductance model developed in Dr. Ehsani's work



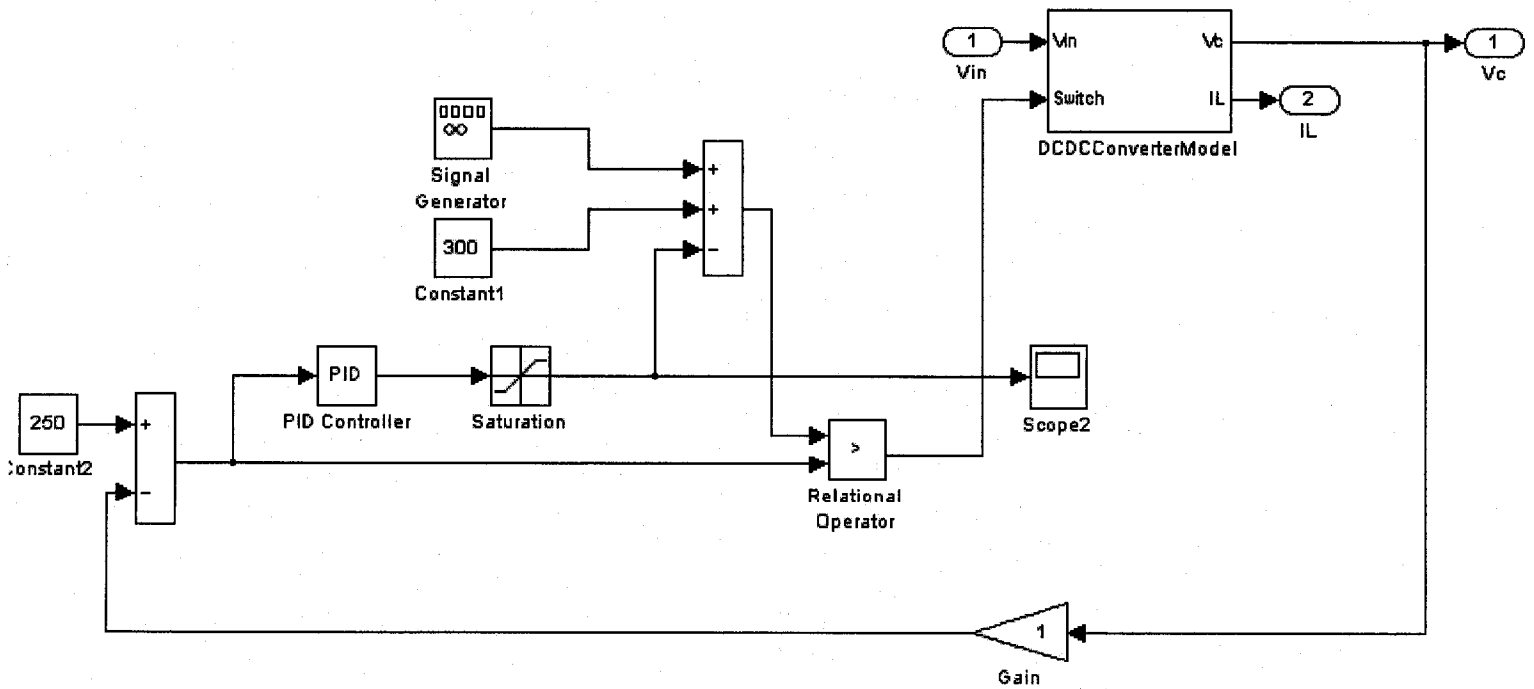
SRM Power chopper Simulink Model



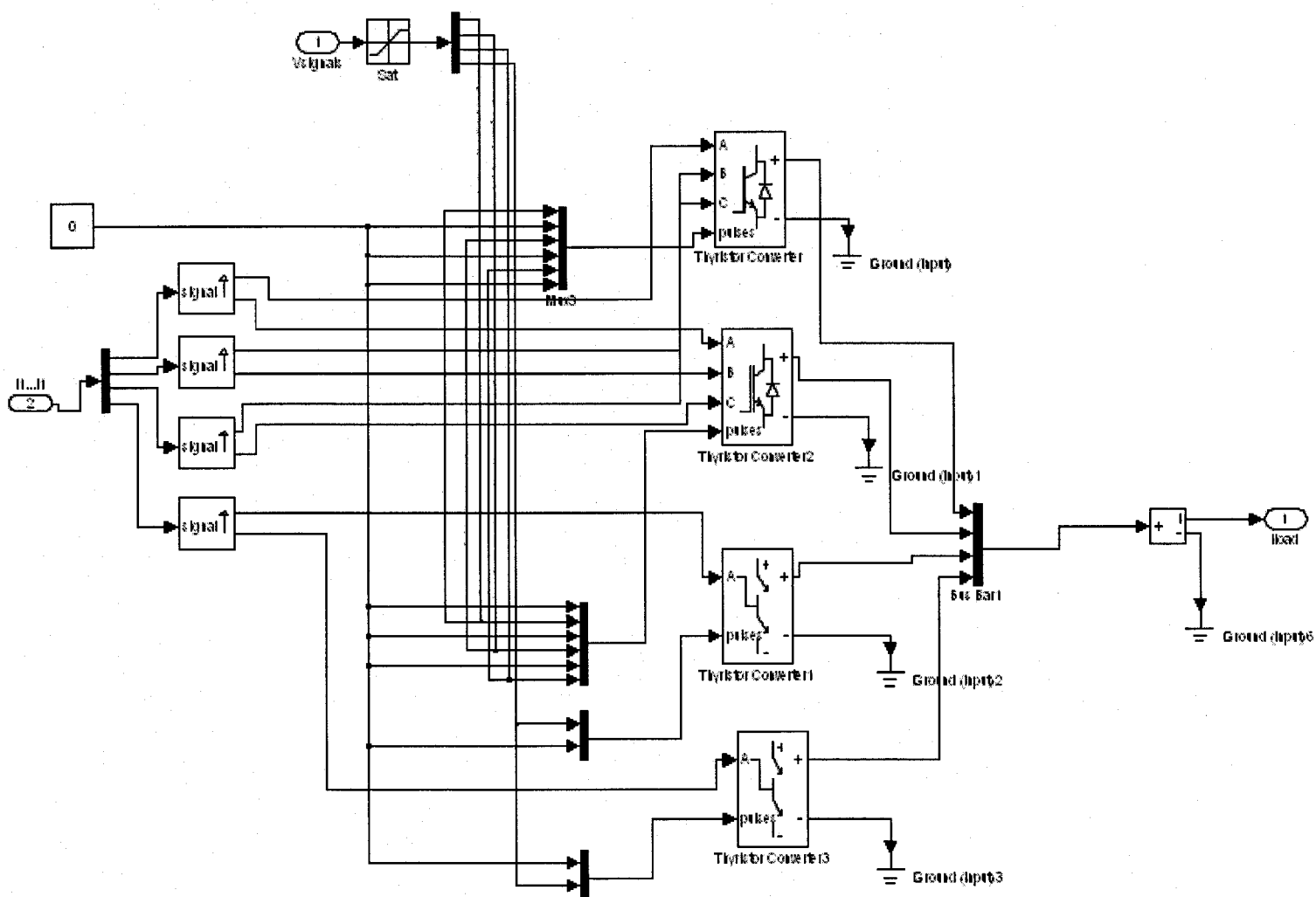
Simulink Mechanical Model



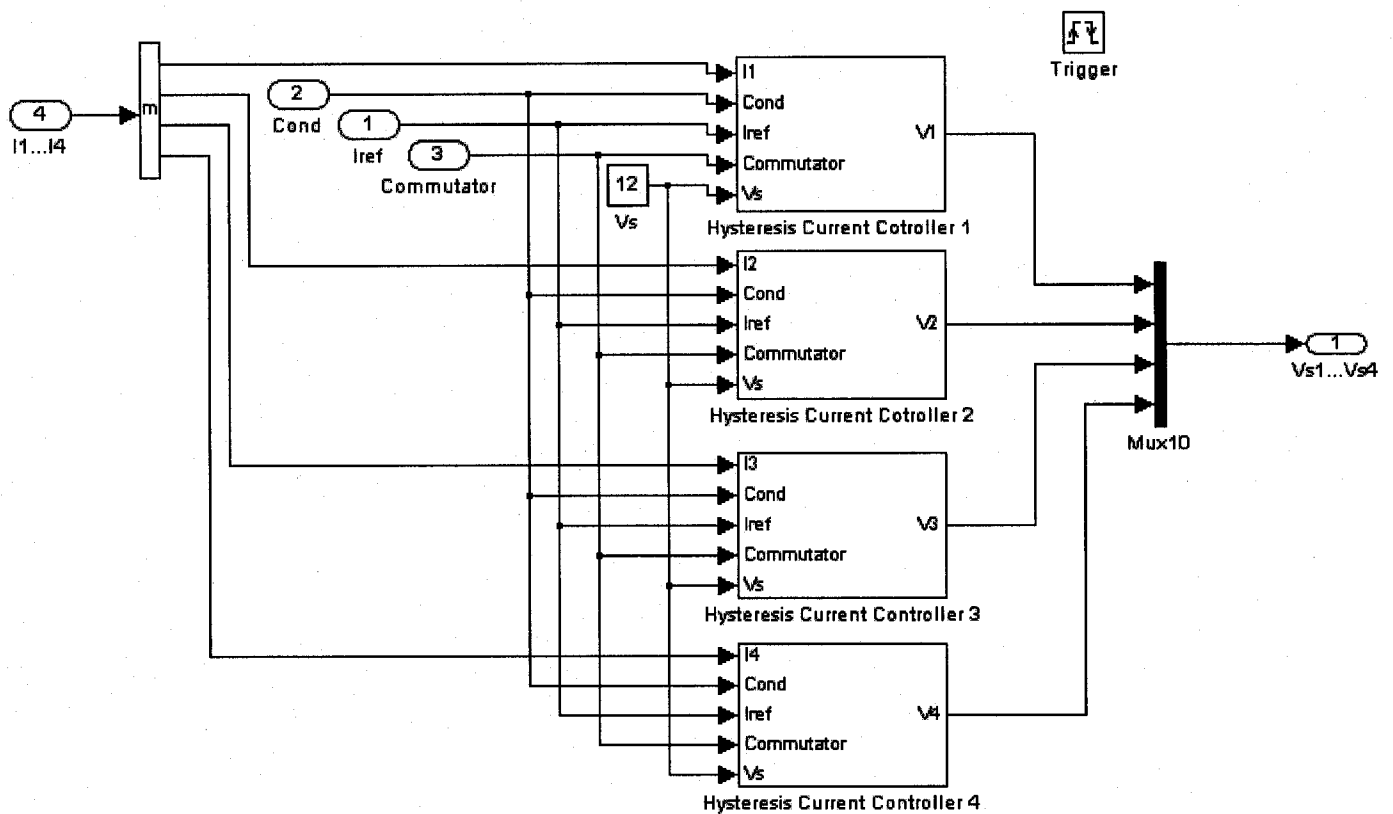
Commutator Angle Simulink Model



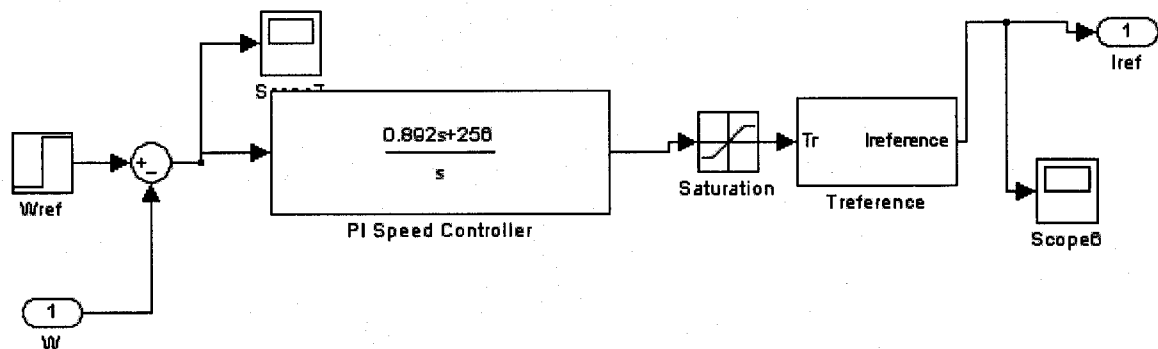
DC/DC Converter Simulink Model



Current Converter Simulink Model



Hysteresis Current Controller Simulink Model



PI Speed Controller Simulink Model

VITA AUCTORIS

NAME: Meranda Salem

PLACE OF BIRTH: Egypt

YEAR OF BIRTH: 1979

EDUCATION: W. D. Low High school, Windsor, Ontario
1995-1997

University of Windsor, Windsor, Ontario
1997-2001, B. A. Sc.

University of Windsor, Windsor, Ontario
2002-2004, M. A. Sc.